Interpreting Inverse Magnetic Fabric in Miocene Dikes From Eastern Iceland

D. Trippanera, M. Porreca, S. Urbani, C. Kissel, A. Winkler, L. Sagnotti, S. Nazzareni, V. Acocella

JGR Solid Earth

RESEARCH ARTICLE
10.1029/2020JB020306

Interpreting Inverse Magnetic Fabric in Miocene Dikes From Eastern Iceland

D. Trippanera[1,2], M. Porreca[3], S. Urbani[1], C. Kissel[4], A. Winkler[5], L. Sagnotti[5], S. Nazzareni[3], and V. Acocella[1]

[1]Department of Sciences, University of Roma Tre, Rome, Italy, [2]King Abdullah University of Science and Technology (KAUST), Thuwal, Saudi Arabia, [3]Department of Physics and Geology, University of Perugia, Perugia, Italy, [4]Laboratoire des Sciences du Climat et de l'Environnement, CEA, CNRS, UVSQ, Gif-sur-Yvette Cedex, France, [5]Istituto Nazionale di Geofisica e Vulcanologia (INGV), Rome, Italy

Key Points:
- Our analyses about the magnetic fabric of the Alftafjordur dike swarm revealed that most of the samples show an inverse magnetic fabric
- The origin of the inverse magnetic fabric is associated with the development of horizontal fractures during the cooling stage of dikes
- It is not straightforward to infer the magma flow direction on deep and old exhumed dikes by using standard low-field AMS measurements only

Supporting Information:
- Supporting Information S1

Correspondence to:
D. Trippanera,
daniele.trippanera@kaust.edu.sa

Citation:
Trippanera, D., Porreca, M., Urbani, S., Kissel, C., Winkler, A., Sagnotti, L., et al. (2020). Interpreting inverse magnetic fabric in Miocene dikes from Eastern Iceland. *Journal of Geophysical Research: Solid Earth*, *125*, e2020JB020306. https://doi.org/10.1029/2020JB020306

Received 30 MAY 2020
Accepted 21 OCT 2020
Accepted article online 29 OCT 2020

Abstract Anisotropy of Magnetic Susceptibility (AMS) is a valid tool to investigate magma flow direction within dikes. However, geometrically inverse magnetic fabric characterized by maximum magnetic susceptibility axis (kmax) perpendicular to the dike wall may complicate the interpretation of flow trajectories. To better understand the nature of this fabric, we present a multiscale study on 19 dikes (383 samples) in the Miocene Alftafjordur volcanic system (Iceland), where 80% of the samples show a geometrically inverse magnetic fabric. We carried out (1) AMS measurements at different magnetic fields and temperatures, along with Anisotropy of Anhysteretic Remanent Magnetization (AARM) analysis; (2) hysteresis loops and FORC diagrams; (3) thin section analysis; (4) structural fieldwork. A variable Ti-content ($0.1 < x < 0.6$, $Fe_{3-x}Ti_xO_4$) titanomagnetite is the main magnetic carrier, and the contribution of the paramagnetic elongated crystals to the magnetic fabric is negligible. Single domain is not the prevailing domain state of the magnetic particles, suggesting that its occurrence cannot be the main cause for the inverse fabric. AMS analysis at different fields and temperatures along with AARM allow us to exclude any mineral phase change of the titanomagnetite across the dike. Nevertheless, kmax is parallel to a diffuse horizontal column-like fracture pattern perpendicularly oriented with respect to the dike strike. This suggests that the Ti-magnetite mineral orientation during dike cooling was affected by the fracture network progressively developing columnar basalts. This study demonstrates that the interpretation of AMS data on old and deep volcanic bodies is not straightforward and observations at different scales are required.

1. Introduction

The Anisotropy of Magnetic Susceptibility analysis (AMS) is a powerful method to study magmatic texture in both extrusive and intrusive magmatic deposits (Cañón-Tapia, 2004; Knight & Waker, 1988; Ort et al., 2015; Tarling & Hrouda, 1993, and references therein). The AMS tensor is geometrically described by an ellipsoid in which the three orthogonal principal axes correspond to the directions where magnetic susceptibility is maximum (kmax), intermediate (kint), and minimum (kmin), with kmax ≥ kint ≥ kmin (Hrouda, 2011). The magnetic lineation is identified by the kmax axis, whereas magnetic foliation is represented by the magnetic plane perpendicular to the kmin axis. In magmatic rocks, AMS analyses are used to infer flow direction, as they give access to the average spatial arrangement of the ferromagnetic, paramagnetic, and diamagnetic mineralogical fractions into the sampled rock. However, the interpretation of AMS results may not be straightforward, as the formation of late mineralogical phases after emplacement could partially or totally overprint the original magnetic fabric (Rochette et al., 1999). Consequently, the interpretation of the AMS results in terms of magmatic trajectories would be altered.

In the last decades, AMS analysis has been widely applied in dikes to infer flow direction and study magma propagation from source to the surface (Knight & Waker, 1988; Poland et al., 2004; Porreca et al., 2006; Soriano et al., 2008). The general model assumes that the shape-preferred orientation of ferrimagnetic grains (e.g., Ti-magnetite) mimics the flow geometry within the dike; that is, the kmax axis is subparallel to the flow direction, and the magnetic foliation is subparallel to the margins or imbricated close to the dike wall (Chadima et al., 2009; Geoffroy et al., 2002). This "normal magnetic fabric" has been observed in basalt containing multidomain (MD) and pseudo-single domain (PSD) magnetite grains.

However, in mafic dikes a magnetic foliation oriented at a high angle (up to orthogonally oriented) with respect to the dike margins is frequently recognized. This is the case of the so-called "anomalous" fabric that shows geometrically inverse (kmax and kmin axes are inverted) or intermediate fabric (kmax and kint or kint and kmin are exchanged). In literature, there are many examples of dike swarms where an important number of dikes show "anomalous" fabric, such as in Oman (Rochette et al., 1991), Ponta Grossa (Brazil, Raposo & Ernesto, 1995), East Greenland (Callot et al., 2001), Rio Ceara´–Mirim (Brazil, Archanjo, 2002), Iceland (Kissel et al., 2010), and Tenerife (Soriano et al., 2008, 2016). In these cases, an "anomalous" fabric has been identified in up to 58% of the investigated dikes (Archanjo, 2002).

Several complicating factors may be responsible for "anomalous" AMS fabrics. The occurrence of single-domain (SD) magnetite (Ferré, 2002; Potter & Stephenson, 1988; Rochette et al., 1992), the "distribution anisotropy" of clusters of magnetic grains (Hargraves et al., 1991; Stephenson, 1994), nonflow-parallel grain alignment by viscous fluid flow (Cañón-tapia & Chávez-Álvarez, 2004; Dragoni et al., 1997), a secondary overprinting of primary flow fabric due to late cooling (Almqvist et al., 2012; Ellwood, 1978; Martin et al., 2019; Mattsson et al., 2011), and the existence of two magma pulses of different composition (Hrouda et al., 2019) or tectonics (Eriksson et al., 2014; Kusbach et al., 2019; Park et al., 1988; Soriano et al., 2007) are among the main established processes that may produce such anomalous fabric. Additionally, due to the different crystallization timing of the minerals within the dike or to metasomatism processes, a composite fabric may also be found. In this case, paramagnetic minerals (early crystallization) are oriented according to the magma flow, whereas ferrimagnetic minerals distribution (later crystallization) reflects the late-stage emplacement and cooling stresses or postemplacement alteration (Silva et al., 2008, 2014).

In such cases, the reconstruction of the magma flow direction is not straightforward. For this, additional magnetic and petrographic techniques must be integrated with and compared to the AMS in order to understand the origin of the anomalous fabrics and correctly interpret the AMS data.

Here we show data obtained by a combination of magnetic anisotropy (AMS and AARM), rock magnetic (hysteresis loops, FORC and Day diagrams, and thermomagnetic curves), petrographic (optical microscope and SEM), and field analyses performed on the exposed Tertiary Alftafjordur dike swarm in Eastern Iceland (Eriksson et al., 2014; Paquet et al., 2007; Urbani et al., 2015; Walker, 1960, 1974, and references therein). We investigated 19 of these dikes, of which only two show a geometrically normal fabric. We analyzed the dikes' fabric at different scales, from mesoscale (outcrop scale) to microscopic (optical and electronic microscopic scale) and magnetic scale (magnetic fabric).

We identified variations of magnetic properties within the same dike along with the influence of the fracture pattern during the cooling stage, demonstrating the difficulties to properly interpret the magnetic fabric in terms of flow direction. The results of this multidisciplinary approach allowed us to obtain insights on the origin of the inverse fabric that can be useful in other similar magmatic contexts.

2. Geological Setting and AMS Studies in Icelandic Dikes

The Eastern margin of Iceland exposes the roots of the rift volcanic successions (mainly lava flows) dated up to 10–12 Ma (K-Ar ages, Moorbath et al., 1968). Recent radiometric dating (K-Ar) of the intruding dikes indicates ages ranging between 9.4 and 10.5 Ma (Kissel et al., 2010), showing that the emplacement of the dikes shortly followed that of the hosting lava flows. These dikes are related to four volcanic systems (viz., Thingmuli, Breiddalur, Alftafjordur, and Reydarfjordur) that are made of basaltic cone sheets (associated with the central volcano) and rift parallel (NNE-SSW oriented) dike swarms 5–10 km wide and 50 km long (Gudmundsson, 1995; Paquet et al., 2007; Urbani et al., 2015; Walker, 1974). The outcropping rocks correspond to a paleo-depth of 1.5 km (Walker, 1960, 1974), even though the lava pile and the intruding dikes continue below the sea level up to 4–6 km of crustal paleo-depth (Gibson, 1983; Robinson et al., 1982). The rift parallel dikes are 4–6 m thick on average but decrease in thickness with altitude (Gudmundsson, 1995; Helgason & Zentilli, 1985; Paquet et al., 2007; Urbani et al., 2015).

To study the magma propagation in such a well-exposed fossil rift zone, the AMS technique has been extensively used as a proxy for magma flow direction since the 1970s. Ellwood (1978) sampled five subvertical dikes in Eastern Iceland. The AMS results were characterized by clustering the anisotropy axes, with kmax

oriented either perpendicular or parallel to the dike plane. In order to better understand such different orientations of the main magnetic axes with respect to the dike plane, Ellwood (1979) performed another detailed AMS study of two near-vertical dikes. In this case, the recurrent near-vertical orientation of kmin axes and horizontal orientations of the kmax axes (perpendicular to the dike margins) were interpreted as evidence of compaction effects due to downward vertical forces exerted by overlying columns. The data were therefore related to secondary processes and not considered representative of the original magma emplacement. These first studies demonstrated that the interpretation of the AMS results of exhumed mafic dikes is not straightforward in terms of magma flow directions when post emplacement processes occur.

Craddock et al. (2008) sampled 13 dikes (153 samples) in both eastern and western Iceland, mostly finding indication for a vertical magma propagation (vertical kmax). However, they highlighted unexpected high values of magnetic anisotropy degree (up to 34% of samples) and orientations of magnetic lineation (12% of samples) along with an anomalous AMS fabric in two dikes from Eastern Iceland. They also found two Ti-magnetite components: one with negligible Ti-content (Tc ~ 580°C) and the other with higher Ti-content (Tc = 180°C); both in the PSD (Pseudo-Single-Domain) grain size range.

Kissel et al. (2010) sampled 27 basaltic vertical dikes (640 samples) from the Reydarfjordur volcanic system to the north of Alftafjordur swarm (Eastern Iceland). They identified three types of magnetic fabrics with well-defined mean principal axes of anisotropy: (1) normal fabric (kmax is vertical and kmin orthogonal to the dike margins) carried by low Ti-content titanomagnetite crystals, (2) inverse fabric (kmax orthogonal to the dike margins and kmin is vertical), and (3) mixed fabric (normal fabric at the margins and the inverse in the center of the dike). The latter is entirely normal after heating the samples at temperatures higher than 400°C. The authors interpreted these two geometrically normal and inverse magnetic fabrics as primary, representing different physical-chemical conditions during the emplacement of the magma, suggesting a vertical extrusion of the magma at the depth of the studied sites.

Eriksson et al. (2011, 2014) performed an AMS study on 12 mafic dikes and at the margins of a quartz-rich composite dike of the Alftafjordur dike swarm. In contrast with previous studies, the authors used kmin instead of kmax to infer the flow direction. In nine of the dikes, they identified a subhorizontal (e.g., 35°–64° inclined in the composite dike) northward magmatic flow, directed away from the central volcano. For the three other dikes they observed a vertical-oriented flow. They suggested that dike propagation in this type of Icelandic volcanic system originated from shallow crustal magma chambers and that the subhorizontal magnetic lineation was the effect of shear tectonic stress.

On the same swarm, the successive integrated field observations and AMS study by Urbani et al. (2015) highlighted prevalent inverse magnetic fabric. Thanks to petro-fabric and other kinematic indicators measured in the field, the same authors suggested a prevalent vertical magma direction, even if they did not discuss the origin of this inverse fabric.

These works demonstrate that, based on AMS studies, there is not a unique interpretation of the magmatic flow directions, also for the same dike swarm (see the case of Alftafjordur). These uncertainties are related to the diffuse occurrence of inverse magnetic fabric in most of the studied dikes and the evolution of different fabrics between the margin and the inner part of the dike.

3. Sampling and Methods

We focused on dikes belonging to the fissure swarm of the Alftafjordur volcanic system as described by Urbani et al. (2015). We sampled a total of 19 dikes at 23 sampling sites along the swarm (Figure 1). The sampling at each site was conducted along a section across the dike with higher sample density at the margins (same procedure of Kissel et al., 2010). We obtained a total of 383 oriented cores extracting two samples from most of the cores. Each sampling site has been labeled with a number (e.g., AL09) followed by the number of the core within the site (e.g., AL0904). When two samples are extracted from the same core, we assigned a letter for each one (A or B). The final code for each sample includes all this information, for example, AL0904A. We measured all the samples in order to describe the magnetic fabric across the dikes and also to investigate the variation of the magnetic properties at the core scale. In order to study the variability of the magnetic fabric along the strike and the height of the dike, one dike was sampled at four sites, with a

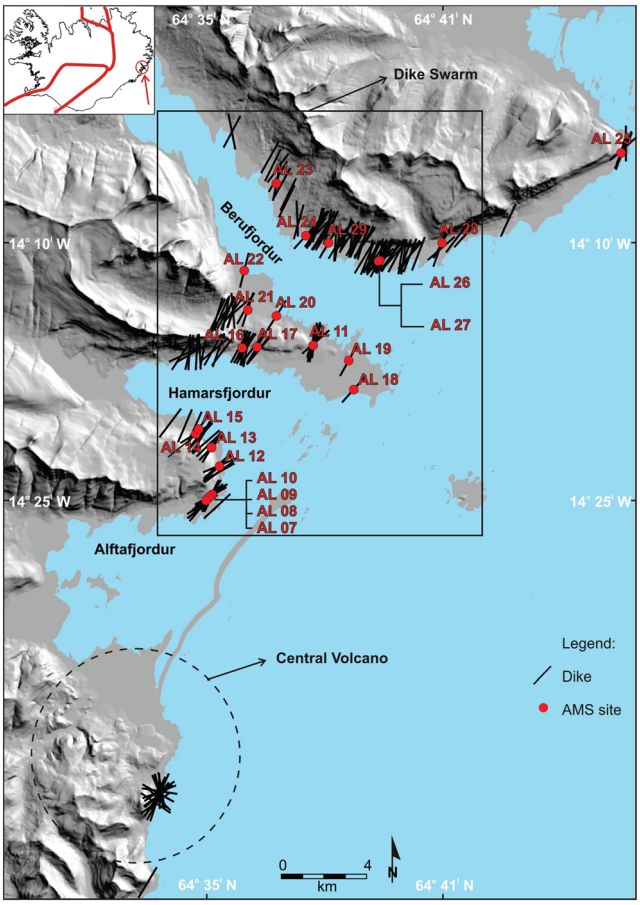

Figure 1. Map of the Alftafjordur dike swarm in Eastern Iceland (see inset). The orientation of the measured dikes in the field along with locations of sampling sites for AMS (e.g., AL26) is indicated. See Urbani et al. (2015) for further details.

50–100 m spacing (sites AL07, AL08, AL09, and AL10) and another dike at two sites with different elevation (sites AL14 and AL15). Further details about sampling are in the supporting information.

3.1. Magnetic Fabric and Rock Magnetic Analysis

Here we describe the aims of each measurement we conducted, while the details of the applied methods and the used instruments can be found in the supporting information. Low-field AMS measurements with field intensity H = 300 A/m were carried out on all the samples using a KLY3S (see supporting information) in order to reconstruct the fabric given by all magnetic grains. Normal, inverse, or intermediate magnetic fabric were identified by comparing the AMS results with the geometry of the dike margins. In order to test any dependence of the magnetic fabric on the applied AF peak field (H), AMS and magnetic susceptibility (k) were also measured at H = 200 A/m and H = 600 A/m (using a MFK1, see supporting information) on three sites (33 samples) characterized by an inverse magnetic fabric (sites AL14, AL22, and AL27).

Following the approach used by Kissel et al. (2010), AMS was also measured in two representative normal and inverse fabric samples (site AL27) after heating the samples in zero field at increasingly higher temperature (20, 200, 400, 500, 550, and 580°C) using H = 200 A/m. This technique was used to detect possible magnetic mineralogical changes upon heating and to investigate their impact on the magnetic fabric.

To better isolate the contribution of ferromagnetic minerals from that of the paramagnetic and diamagnetic minerals, we also carried out analyses of the Anisotropy of Anhysteretic Remanent Magnetization (AARM) (Chadima et al., 2009; Jackson et al., 1988; McCabe et al., 1985). These measurements were performed by superimposing a 0.05 mT DC field to a 30 mT AF field along the 12 directions in the scheme "A" of the Agico LDA-3A AF demagnetiser, equipped with a AMU-1A anhysteretic magnetizer. A tumbling AF field of 40 mT was applied before each ARM step. Eight samples (four samples for the two sites AL09 and AL28) were selected for AARM analysis. Moreover, the variation of magnetic susceptibility with temperature was analyzed in free air for six selected samples, four from sites with inverse fabric (sites AL14 and AL28), and two from sites with normal fabric (sites AL14 and 27). This aimed at identifying and comparing the main magnetic carriers according to their estimated Curie temperatures, in addition to their magnetic behavior with temperature, for both inverse and normal fabrics. Field dependence of magnetic susceptibility (k) in the field range of 2–700 A/m was also measured for nine samples (sites AL14, AL22, and AL27) characterized by both normal and inverse fabric. The variation of k with the applied field (k_{HD}) is particularly useful to estimate the Ti-content of titanomagnetite (Chadima et al., 2009; De Wall, 2000).

In order to characterize the magnetic domain state (single, pseudo-single, and multidomain) giving access to the magnetic grain size, we performed hysteresis analyses and First Order Reversal Curves (FORCs) on representative samples, both from normal and inverse fabrics (sites AL14, AL17, and AL27; i.e., Pike et al., 1999, 2001; Rochette et al., 1992; Roberts et al., 2000). Moreover, the variation of hysteresis parameters was investigated upon heating in order to determine the thermal distribution and stability of different populations of magnetic domains (Kissel et al., 2010).

3.2. Petrographic Analysis

Mineral texture and assemblage along with chemical composition of both phenocrysts (e.g., plagioclase and pyroxene) and opaque minerals (e.g., Ti-Fe oxides) were studied for four representative sites (AL09, AL14, AL22, and AL27) in 13 thin sections using optical and scanning electron microscope (SEM). The studied samples are representative of either normal or inverse magnetic fabric. Image analysis focused on

defining the texture and orientation of phenocrysts, and opaque minerals (magnetic minerals) were used to investigate the relationships between petro- and magnetic fabric, in a similar approach as used by Bascou et al. (2005) and Hastie et al. (2011). To do this, we selected samples showing both AMS normal and inverse fabric that were placed either close to the dike margins or in the central portion of the dikes. The petro-fabric of the nonopaque grains also gives independent constraints on the magma flow direction because the major axes of the grains (e.g., phenocrysts) align parallel to the direction of any laminar flow.

3.3. Field Analysis

We measured with a standard magnetic compass (paying attention to minimize the magnetic deviation) the joint orientations along seven dikes (a total of 11 sites: AL07, AL08, AL09, AL10, AL14, AL15, AL16, AL17, AL22, AL27, and AL28) and obtained field and drone images of some of them to reconstruct the distribution of the joints within the dike. These data were then compared to the magnetic results in order to check whether cooling or tectonic processes could control the AMS fabric. A summary of the samples where multiple analyses have been carried out is shown in Table S1.

4. Results

4.1. Magnetic Fabric

4.1.1. Low-Field AMS

The dikes of the swarm are NNE to NE oriented (Figure 2; mean direction N48°; see Urbani et al., 2015, for further details). The orientations of the principle axes of magnetic susceptibility are homogeneous, considering the overall 383 measured samples. In particular, kmax is generally subhorizontal and perpendicular to the dike swarm (Figure 2a; Dec. N308°, Inc. 8° with 37° and 23° confidence angles, respectively), kint is subhorizontal and parallel to the dike swarm (Figure 2b; Dec. N217°, Inc. 6° with 36° and 30° confidence angles, respectively), whereas kmin is mainly vertical (Figure 2c, Dec. N91°, Inc. 81° with 30° and 24° confidence angles, respectively). This configuration is commonly defined as geometrically inverse magnetic fabric, and it is represented by about 80% of the measured samples. The remaining 20% of the samples show intermediate or normal magnetic fabric.

The overall bulk susceptibility (k) is relatively high, ranging from $9.2{\cdot}10^{-3}$ to $1.6{\cdot}10^{-1}$ SI with an average value (kmean) of $6.0{\cdot}10^{-2}$ SI (Figure 2d and Table 1). The corrected anisotropy degree values (Pj) are also relatively high and range between 1.0 and 1.6, with most of the samples close to the average value of 1.075 (Figure 2e and Table 1). No relationships are found between the anisotropy degree (P) and bulk susceptibility (k), as shown in Figure 2d. The shapes of the ellipsoids span through the whole range from oblate to prolate shapes. Moreover, 10 outlier cores present very high foliation values ($F > 1.2$) corresponding to oblate AMS ellipsoids associated with very high anisotropy degrees ($Pj > 1.3$).

At the site level, the average Pj value is below or equal to 1.1, and only in two sites we observed a higher Pj (Figure 2f, Table 1). Kmean is around $4{\cdot}10^{-2}$ SI, ranging between $2{\cdot}10^{-2}$ SI and $6{\cdot}10^{-2}$ SI for most of the sites (Figure 2g).

Regarding the orientation of the magnetic axes in each single site, different types of magnetic fabric were observed (Figure S1 and Table 1; Trippanera et al., 2020):

- Two sites with normal fabric: kmax is within the dike plane with different dips and kmin is subhorizontal and perpendicular to the dike plane (sites AL12 and AL16).
- One site with intermediate fabric: kmax is subhorizontal and kmin subvertical both within the dike plane (site AL11).
- Four sites with mixed fabric consisting of samples with both normal and inverse fabric across the dike width (sites AL14, AL23, AL25, and AL27).
- Sixteen sites with inverse fabric: kmax is subhorizontal and perpendicular to the dike plane, kmin either subvertical or subhorizontal within the dike plane (sites AL07, AL08, AL09, AL10, AL13, AL15, AL17, AL18, AL19, AL20, AL21, AL22, AL24, AL26, AL28, and AL29).

When the same dike is sampled at different points along the strike (e.g., sites AL07 to AL10 and AL14 to AL15, Table 1), a consistent inverse fabric is observed.

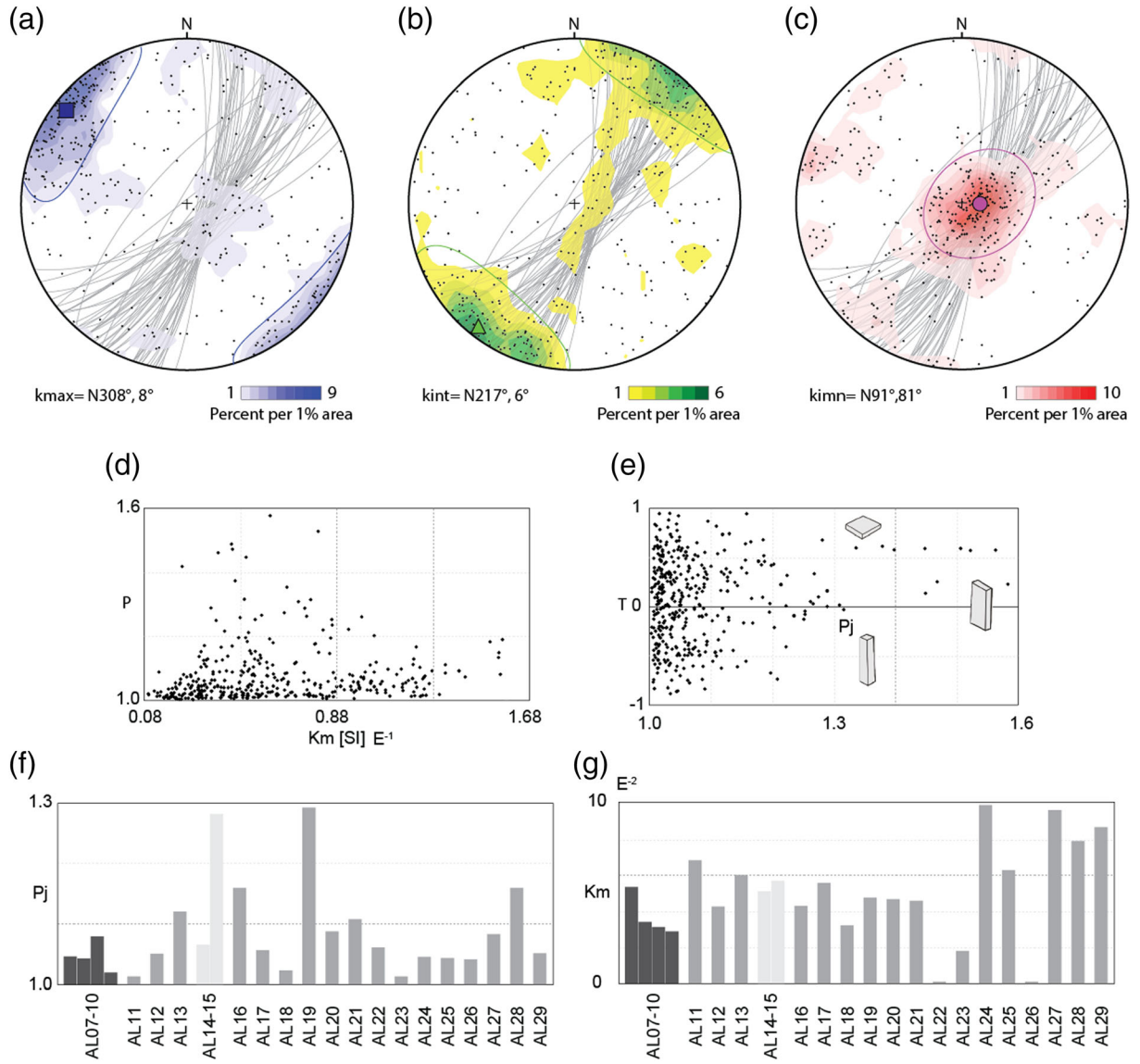

Figure 2. Stereoplot (on the lower hemisphere) showing the orientation of (a) kmax), (b) kint, and (c) kmin axes (black dots) obtained from all AMS measurements with H = 300 A/m. The median value and the relative α 95 confidence ellipse obtained by the Anisoft software (Chadima & Jelínek, 2008) are also indicated for each axis. The color scale illustrates the density of points (that are the magnetic axes) expressed by using the 1% area method (%value = $n(100)/N$ where n is the number of points falling within an area of the plot and$N$is the total number of points) obtained by Stereonet software (Allmendinger et al., 2013; Cardozo & Allmendinger, 2013). Dike planes are plotted in gray. For each sample is also plotted (d) P versus Km and (e) T versus Pj. Histograms of median Pj (f) and Km (g) values for each sampled site (Table 1). Histogram bars for multiple sites from the same dike are closer to each other and colored with dark (sites AL07, AL08, AL09, and AL10) and light (sites AL15 and AL16) gray.

In the next paragraphs, we report the details of AMS results from four representative dikes characterized by inverse and mixed fabrics. In each case we show the sampling positions within the dike, the distribution of the Pj and T along the sampling transect and the equal-area projection of the principal AMS axes (kmax and kmin). The equal-area projections of the magnetic axis for all sites are reported in Figure S1 and raw data accessible in Trippanera et al. (2020) (data set repository).

4.1.1.1. Inverse Fabric

Sites AL28 and AL22 are examples of dikes characterized by inverse magnetic fabric.

At site AL28 we drilled eight samples across the dike (Figure 3a). The mean anisotropy degree and kmean are among the highest of the sampled dikes (highest Pj = 1.262, mean Pj = 1.159; mean, kmean = $7.91{\cdot}10^{-2}$ SI; Figures 2f, 2g, and Table 1). Across the dike, Pj values are lower close to the western margins and higher

Journal of Geophysical Research: Solid Earth

10.1029/2020JB020306

Table 1

List of the Sampled Sites Showing for Each Site: Location in Latitude (Lat.) and Longitude (Long.), Number of Cores (N), Median Value of Magnetic Parameters (Km, L, F, T, and Pj, see Supporting Information), Median Azimuth Angle (D) and Inclination (I) of the Three Principal Magnetic Axes, Dike Orientation, and Overall Geometric Fabric Obtained by AMS Measurements

	Coordinates												
AMS site	Lat.	Long.	*N*	Km	L	F	T	Pj	Kmax (D, I)	Kint (D, I)	Kmin (D,I)	Dike attitude (strike, dip)	Fabric
AL07	64°35′59.92″N	14°25′8.61″W	17	5.37 (0.932)	1.014 (0.018)	1.031 (0.024)	0.392 (0.354)	1.047 (0.043)	314, 5	224, 3	104, 84	232, 88	Inverse
AL08	64°35′58.17″N	14°25′13.79″W	16	3.38 (1.17)	1.027 (0.024)	1.014 (0.009)	−0.114 (0.514)	1.044 (0.030)	312, 8	43, 9	180, 78	52, 78	Inverse
AL09	64°35′54.74″N	14°25′22.19″W	14	3.13 (0.877)	1.030 (0.014)	1.046 (0.031)	0.178 (0.208)	1.079 (0.045)	302, 7	34, 16	190, 73	44, 77	Inverse
AL10	64°35′51.21″N	14°25′31.38″W	19	2.87 (1.31)	1.008 (0.006)	1.012 (0.009)	0.109 (0.461)	1.021 (0.011)	320, 7	57, 46	223, 43	49.82	Inverse
AL11	64°39′34.09″N	14°18′33.71″W	15	6.85 (1.49)	1.006 (0.003)	1.008 (0.003)	0.160 (0.344)	1.014 (0.004)	32, 7	302, 5	177, 82	19, 76	Intermediate
AL12	64°36′41.69″N	14°24′35.96″W	12	4.27 (2.23)	1.030 (0.014)	1.018 (0.013)	−0.245 (0.456)	1.051 (0.016)	148, 74	243, 1	333, 16	67, 75	Normal
AL13	64°37′10.66″N	14°24′58.85″W	12	6 (1.85)	1.029 (0.023)	1.082 (0.084)	0.285 (0.416)	1.120 (0.115)	138, 2	229, 14	41, 76	211, 86	Inverse
AL14	64°37′33.01″N	14°25′51.53″W	18	5.12 (0.914)	1.026 (0.019)	1.038 (0.024)	0.173 (0.286)	1.066 (0.042)	297, 11	29, 11	162, 75	58, 75	Mixed
AL15	64°37′40.27″N	14°25′39.40″W	10	5.68 (1.56)	1.096 (0.052)	1.160 (0.128)	0.145 (0.377)	1.281 (0.175)	301, 15	210, 2	112, 75	34, 80	Inverse
AL16	64°39′38.19″N	14°22′45.09″W	13	4.29 (0.780)	1.056 (0.037)	1.093 (0.027)	0.271 (0.360)	1.159 (0.036)	197, 22	65, 60	296, 20	24, 75	Normal
AL17	64°39′38.03″N	14°21′52.32″W	17	5.59 (1.69)	1.016 (0.013)	1.039 (0.032)	0.379 (0.326)	1.057 (0.042)	337, 4	246, 12	85, 78	16, 79	Inverse
AL18	64°38′22.92″N	14°16′22.39″W	12	3.21 (0.963)	1.012 (0.007)	1.010 (0.007)	−0.098 (0.279)	1.023 (0.014)	284, 46	172, 20	66, 37	42, 75	Inverse
AL19	64°39′07.03″N	14°16′32.26″W	14	4.73 (1.38)	1.085 (0.062)	1.178 (0.119)	0.356 (0.223)	1.291 (0.188)	312, 9	220, 11	79, 76	29, 80	Inverse
AL20	64°40′23.07″N	14°20′36.07″W	14	4.69 (0.807)	1.058 (0.020)	1.026 (0.015)	−0.392 (0.166)	1.088 (0.034)	324, 12	230, 21	82, 66	32, 76	Inverse
AL21	64°40′35.11″N	14°22′15.37″W	15	4.59 (1.42)	1.021 (0.019)	1.078 (0.081)	0.307 (0.473)	1.108 (0.109)	121, 2	211, 12	23, 78	18, 84	Inverse
AL22	64°41′35.49″N	14°22′17.67″W	18	0.107 (1.59)	1.033 (0.020)	1.027 (0.017)	−0.087 (0.398)	1.062 (0.030)	311, 3	221, 10	56, 79	14, 77	Inverse
AL23	64°43′43.43″N	14°20′1.95″W	24	1.81 (0.476)	1.009 (0.007)	1.005 (0.003)	−0.164 (0.432)	1.014 (0.009)	240, 24	332, 5	72, 65	11, 81	Mixed
AL24	64°42′21.17″N	14°18′30.76″W	28	9.88 (2.07)	1.023 (0.015)	1.022 (0.015)	0.007 (0.377)	1.046 (0.024)	146, 4	55, 13	252, 76	222, 71	Inverse
AL25	64°43′49.83″N	13°59′33.16″W	20	6.30 (1.67)	1.015 (0.009)	1.028 (0.019)	0.212 (0.342)	1.045 (0.025)	353, 21	97, 31	235, 51	16, 77	Mixed
AL26	64°41′35.28″N	14°14′15.35″W	15	0.105 (1.53)	1.019 (0.011)	1.021 (0.014)	0.037 (0.349)	1.041 (0.023)	278, 6	182, 42	14, 48	49, 81	Inverse
AL27	64°41′34.25″N	14°14′20.30″W	26	9.60 (4.68)	1.056 (0.048)	1.022 (0.017)	−0.230 (0.535)	1.083 (0.064)	298, 30	34, 10	139, 59	41, 78	Mixed
AL28	64°41′54.78″N	14°10′30.78″W	9	7.91 (1.38)	1.073 (0.049)	1.079 (0.040)	0.098 (0.210)	1.159 (0.093)	111, 8	21, 3	271, 82	38, 74	Inverse
AL29	64°42′07.70″N	14°17′12.58″W	24	8.64 (3.19)	1.022 (0.018)	1.027 (0.021)	0.031 (0.387)	1.052 (0.035)	283, 61	105, 29	15, 1	30, 74	Inverse

Note. Sites AL07-08-09-10 and AL14-15 belong to the same dike. Km is expressed in 10E-2.

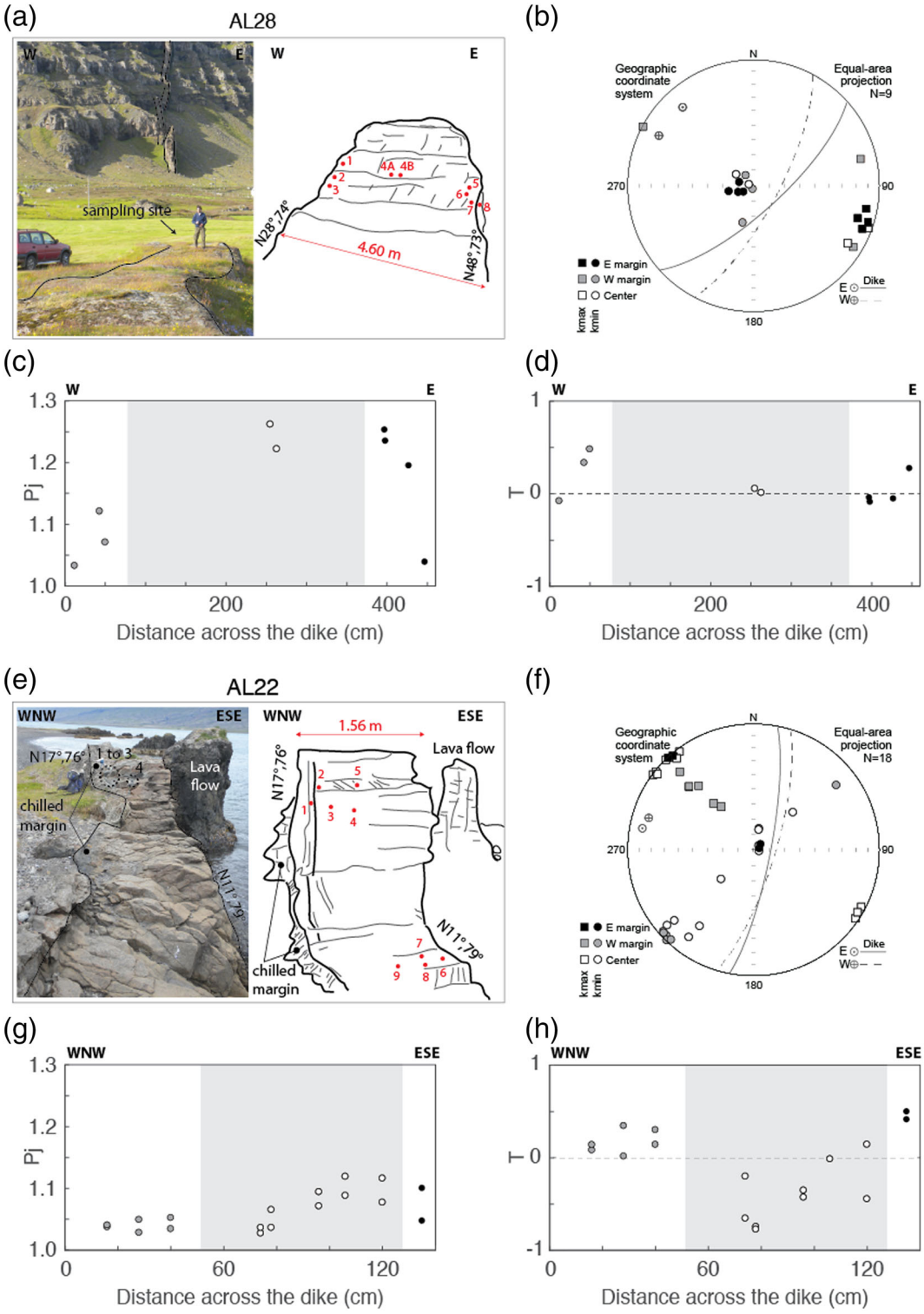

Figure 3. AMS results at sites AL28 and AL22. Picture and sketch of the sampled sites (a) AL28 and (e) AL22 showing the location of each core (red dot) and their assigned number. Stereoplot (lower hemisphere projection) of kmax and kmin axes obtained by AMS measurements with H = 300 A/m for cores close to the western (gray) and eastern (black) dike margins and in the dike center (white) at site (b) AL28 and f AL22. When two samples are extracted from the same core, both of them are plotted. Symbols of the eastern (E) and western (W) dike margins' planes along with the relative poles are indicated at the bottom right of the stereoplots. Variations of Pj and T across the dike at sites (c–d) AL28 and (g–h) AL22. Symbols' colors are the same as the stereoplot. When two dots are at the same distance from the dike margin, they represent both specimens obtained from the same core. Light gray background highlights the dike center.

in the inner portion of the dike (Figure 3c). Most of the samples show triaxial ellipsoids (T close to zero, Figure 3d) with a small scatter of each axis: kmax is subhorizontal and perpendicular to both dike margins; kmin is vertical in the average dike plane (Figure 3b, Table 1).

At site AL22 the dike margins are well-defined, and the chilled margin is still visible where the host rock (lava flows) is preserved (i.e., western margin). We drilled nine cores across the dike obtaining a total of 18 samples (Figure 3e). The mean Pj value is similar to the one obtained from most of the sampled dikes (Pj = 1.062; Figure 2f and Table 1), but kmean is one of the lowest ($0.107 \cdot 10^{-2}$ SI; Figure 2g and Table 1).

Across the dike, relatively low Pj values were found for the samples close to the western margin where the chilled margin is preserved (Figure 3e). The anisotropy degree becomes higher toward the eastern margin (Table 1; Figure 3g). The shape of the ellipsoids is oblate at the margins (T is positive) and prolate in the inner part (T is negative, Figure 3h). At the center and at the eastern margin, the kmax axes are subhorizontal and oriented at a high angle with respect to the dike plane, whereas the kmax dip increases toward the western margin (Figure 3f). To summarize, the inverse magnetic fabric sites are characterized by high Pj values and shapes of the ellipsoids varying from moderately oblate to prolate. Moreover, when the chilled margin is preserved (e.g., AL22), we may observe a variation in the anisotropy degree from the margin to the center and a change of the ellipsoid shape from mostly oblate at the margin to mostly prolate in the center (Figure 3h). This, in some cases, can be also associated with a change in the dip of the kmax axis from subhorizontal at the center to oblique toward the margin of the dike.

4.1.1.2. Mixed Fabric

Here we provide the two most representative examples of mixed fabric that are the dikes sampled at sites AL27 and AL14. At site AL27 (Figure 4; see also Urbani et al., 2015, and Figure S6), the western margin of the dike is well defined by the contact with the host rocks, whereas the opposite margin is not preserved. We drilled 13 cores (for a total of 26 samples) across the dike among which three (six samples) in the chilled western margin (Figure 4a). Overall, the mean Pj value is similar to the majority of the sampled dikes (1.083; Figure 2f and Table 1), but kmean is one of the highest ($9.60 \cdot 10^{-2}$ SI; Figure 2g and Table 1).

The observed magnetic fabrics across the dike can be separated into three groups corresponding to the different positions within the dikes: the western margin (samples 1 to 3), a transitional zone (samples 4 to 6), and the inner group including the nonpreserved eastern margin (8 to 13). The samples collected close to the western margin are characterized by low Pj (Pj = 1.020), whereas the samples from the inner part of the dike are characterized by higher Pj (Pj = 1.124). The "transition" group, between the western margin and the inner part of the dike, is characterized by intermediate Pj (in yellow in Figure 4c and Table 1).

The T shape parameter indicates the prevalence of oblate ellipsoids for the samples close to the western margin, and a prevalence of prolate shapes for the other samples. This difference is reflected also in the orientation of the principal susceptibility axes. In the high Pj samples from the inner part of the dike, kmax is perpendicular to the dike walls (i.e., inverse fabric), whereas in the low Pj samples of the western margin, kmax is vertical within the dike plane (i.e., normal fabric). The transition group shows both normal and inverse fabric, also for different samples from the same core (e.g., core AL2704A and AL2704B).

The dike sampled at the site AL14 shows a well-defined contact with the host-rocks only at the western margin. We sampled 12 cores across the dike width (for a total of 18 samples; Figure 4e). The overall anisotropy degree is similar to the majority of the sites (mean Pj = 1.066, Figure 2f and Table 1), though a second site in the same dike (AL15) shows one of the highest anisotropy degrees (Pj = 1.281). The average susceptibility kmean (kmean = $5.12 \cdot 10^{-2}$ SI) is similar to values measured in most of the dikes and is homogeneous for both sites of the same dike (AL14 and AL15).

Across the site AL14, two groups of samples can be distinguished on the basis of their magnetic properties. The samples close to the eastern margin (1 and 2) have higher Pj than the samples from the inner part of the dike (Figure 4g and Table 1). Most of the AMS ellipsoids are oblate all across the dike with a few triaxial ones at the center. Differently from the eastern margin, the western one is characterized by triaxial or prolate ellipsoids (Figures 4g and 4h). As for site AL27, the high Pj samples are characterized by a kmax perpendicular to the dike plane (i.e., inverse fabric), whereas in the low Pj samples the kmax is almost vertical in the dike plane (i.e., normal fabric) (Figure 4f). For AL14 case most of the normal fabric samples are located in the central portion of the dike.

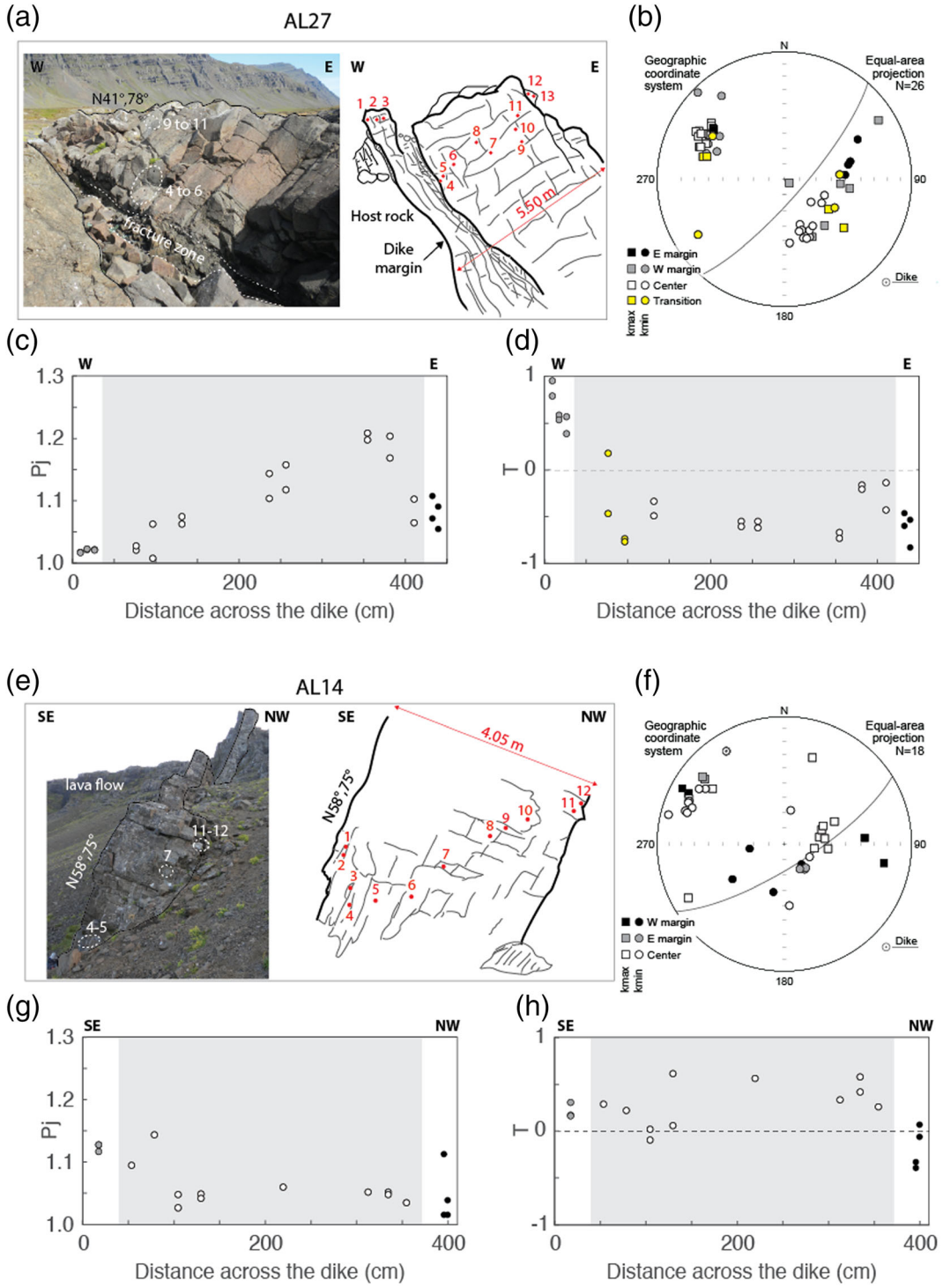

Figure 4. AMS results at sites AL27 (a–d) and AL14 (e–h). Refer to Figure 3for symbology. In dike AL27 the transition group is indicated in yellow. In dike AL14 samples from the eastern and western margins are in gray and black, respectively. The dike plane in the stereo plots indicates the mean dike strike.

To summarize, the mixed fabrics are made of a mixture of normal and inverse fabrics depending on the position of the samples within the dike (close to the margin or in the inner part). The high Pj samples are typically associated with inverse magnetic fabric, whereas the relatively low Pj samples have a normal magnetic fabric. The two examples described in detail here are opposite in their organization, with a normal magnetic

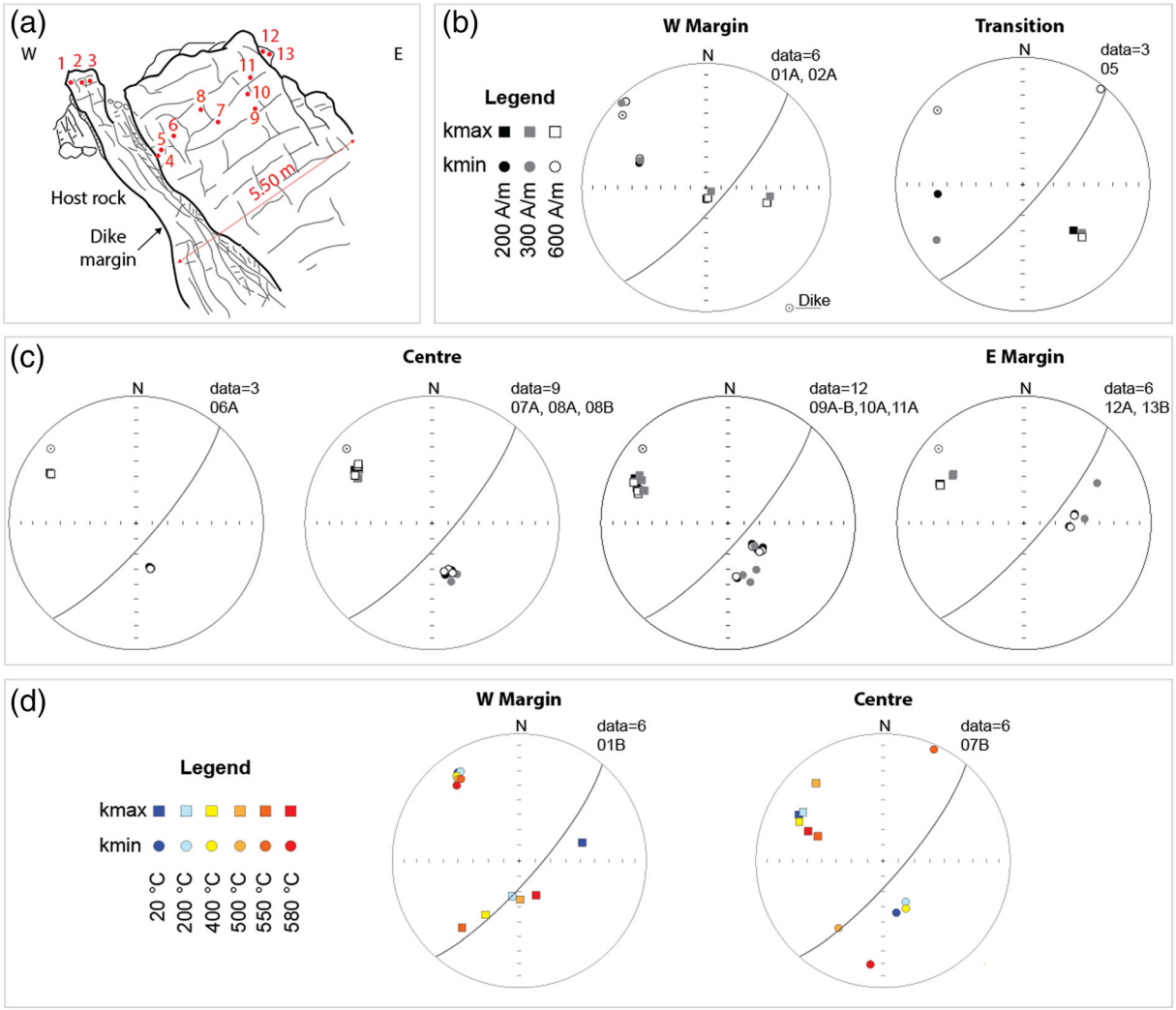

Figure 5. AMS results obtained at different magnetic fields and after heating to different temperatures for the site AL27. (a) Sketch of the sampling site showing the location of each core (red dot) with their assigned number. Stereoplot (lower hemisphere projection) of the kmax (squares) and kmin (circles) axes at different magnetic fields for cores extracted (b) close to the western dike margin and (c) at the center and at the eastern margin. (d) Stereoplot of AMS analysis at different temperatures for two selected cores.

fabric at the margin and an inverse fabric at the center in dike AL27, and the opposite in dike AL14. A transition zone may be also present between the margin and the inner part of the dike, such as at dike AL27.

4.1.2. AMS Variations With Field and Temperature

The results obtained by AMS at different applied fields and temperatures can be summarized examining the case of dike AL27, where both normal and inverse magnetic fabrics coexist (Figure 5). In this case, we classified the AMS data obtained at different applied fields in the same three groups as identified with the low-field experiment (H = 300 A/m), that is, the margin, the transitional zone (Figure 5b), and the inner group (Figure 5c). The AMS data obtained at 200 and 600 A/m are very similar to those obtained at 300 A/m, even if some small angle variations (<10°) in the orientation of the kmax and kmin are recognized for the margin and transition samples. Regarding the shape parameters (not shown in figure), we observed that the variation from oblate at the margin to prolate shapes in the inner part of the dike is confirmed also at fields of 200 and 600 A/m.

The same experiment was conducted on the other dike characterized by a mixed fabric (site AL14) and on a dike with an inverse fabric (site AL22). A general agreement among results obtained from AMS measurements at different fields is also observed for these two sites. In particular, site AL22 shows very well

clustered kmax and kmin (with kmin less clustered at the dike center) axes confirming the occurrence of the inverse fabric at all applied fields (Figure S2).

Due to the limited number of samples, AMS was measured after heating at different temperatures for only two samples of dike AL27 (Figure 5d): one sample from the dike margin showing a normal fabric and one from the dike center showing an inverse fabric. In the normal fabric sample, kmax remains in the dike plane, with a significant variation (up to 40°) in its plunge after heating, whereas the kmin remains well clustered perpendicular to the dike without any plunge variation. In the inverse fabric, kmax remains well clustered and orthogonally oriented with respect to the dike plane. Kmin is overall well clustered on the dike plane. Also, the shape of the AMS ellipsoids does not significantly change at different temperatures (not shown in figure).

In all cases we have therefore not recognized any significant field- or temperature-related variation in the AMS data, differently from Kissel et al. (2010).

4.1.3. AARM Results

All the samples considered for the AARM analysis are characterized by inverse AMS fabrics (H = 300 A/m), except for one sample from the margin of dike AL28 (sample AL2801A) characterized by a fabric intermediate between normal and inverse (Figure S3). The AARM ellipsoid axes are not as well grouped as those of the AMS ellipsoid, but either they continue to show an overall inverse fabric or they change into a not well-defined fabric with both ARM max and ARM min axes out of the dike plane. Among the eight analyzed samples, only one (AL0907A) shows a possible change from AMS inverse to AARM normal fabric (the angle between the dike direction and the ARM max is lower and the ARM min is perpendicular to the dike).

In the case of sample AL2801A, ARM max is horizontal, parallel to the dike plane, therefore still in a normal fabric configuration. We also observed a general decrease of Pj between the AMS and the AARM at site AL09, while at site AL28 the most remarkable effect is the inversion of all the shape parameters from oblate to prolate and vice-versa.

4.2. Rock Magnetism

4.2.1. Thermomagnetic Curves

We measured six k versus temperature (T) curves (Figure 6), selecting samples with both inverse (A1402B, AL2801A, AL2803A, and AL2806A) and normal fabric (AL1409B and AL2704A). We recognized two types of susceptibility behavior. The first type is represented by the sample AL2704, showing an almost reversible heating and cooling temperature cycle. In this case, we observe a gradual increase of the susceptibility up to ca. 500°C and a strong decrease around 500 and 580°C (Figure 6f). This behavior can be associated with the presence of magnetite (Fe_3O_4) or low-Ti content titanomagnetite ($Fe_{3-x}Ti_xO_4$ with a Curie temperature Tc ~ 510°C (TM10, x ~ 0.10) (Dunlop & Özdemir, 1997).

The rest of the samples show a more complicated thermomagnetic behavior characterized by irreversible curves. In particular, we observe an increase in the susceptibility at relatively low temperature with a Hopkinson-type (Hopkinson, 1889) peak between 100 and 250°C. The susceptibility then decreases abruptly between 250 and 450°C. A second phase is also present and disappears between 450 and 550°C (Figures 6a, 6b, and 6e). Finally, the last decrease of susceptibility is accomplished at 600°C, probably due to the presence of titano-hematite, possibly resulting from the oxidation of the magnetic phases during heating. This complex thermomagnetic behavior has been prevalently recognized in all inverse fabric samples, as well as in one normal sample (AL1409B). This type of curve indicates the occurrence of at least two groups of titanomagnetites with variable Ti content in both normal and inverse samples: the low-temperature decrease of susceptibility may be linked to Ti-rich magnetites ($Fe_{3-x}Ti_xO_4$ with x ~ 0.6; TM60, Dunlop & Özdemir, 1997); the high-temperature decrease of susceptibility may be typical for Ti-poor titanomagnetites (x ~ 0.10, TM10).

4.2.2. Field Dependence of Magnetic Susceptibility

Field dependence of magnetic susceptibility is rather variable from samples of different sites as well as for the same site and the same core (i.e., AL1411A and AL1411B), testifying important compositional variations also at the core scale. In fact, the magnetic susceptibility variation (k_{Hd}) ranges from 0% up to 11% (Figure S4), with the maximum value obtained from the inverse fabric sample AL1411B, for which noticeable field dependence was measured (k_{Hd} = 11.2%). The variation of k_{Hd} reflects a wide variation of Ti content in

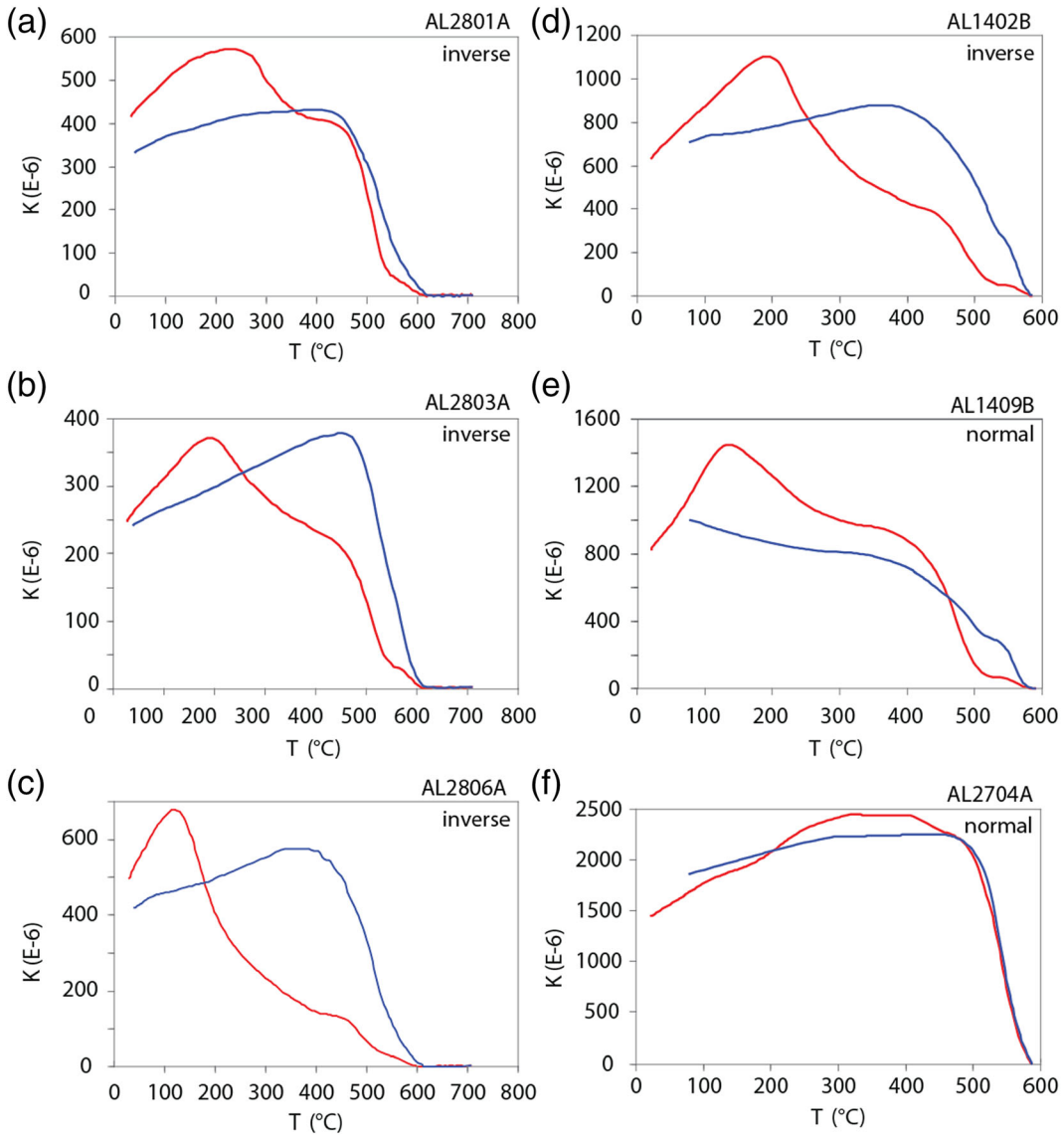

Figure 6. Thermomagnetic curves for samples from three different sites (AL14, AL27, and AL28) characterized by either normal or inverse samples. Heating and cooling curves are in red and blue, respectively.

titanomagnetite, as also indicated by thermomagnetic curves, with maximum k_{Hd} values typical for Ti-rich titanomagnetite (Chadima et al., 2009; Hrouda, 2011).

4.2.3. Hysteresis Parameters and FORC Diagrams

We analyzed the hysteresis loops of 10 samples characterized by normal or inverse AMS magnetic fabric and belonging to three sites (AL14, AL17, and AL27). The ratios Mrs/Ms versus Bcr/Bc were plotted in a Day plot and compared to theoretical magnetite (Day et al., 1977; Dunlop, 2002; Figure 7a). In the Day plot, the samples fit quite well the trend lines for a mixture of SD and MD magnetite particles, even if Ti-rich composition should influence the distribution of points in the plot, especially approaching the SD and MD ends (Dunlop, 2002). As a general trend, the samples with inverse magnetic fabric show a higher contribution of MD grains, with respect to the normal ones; thus, it is possible to argue that inverse magnetic fabric is not connected to the presence or abundance of SD particles.

The FORC diagrams obtained at room temperature for samples AL1402B (inverse) and AL1409B (normal) highlight magnetic components carried by MD magnetic grains (Roberts et al., 2000) (Figure 7b). In the sample AL1702A (normal) the double peak suggests the coexistence of MD and SD low coercivity

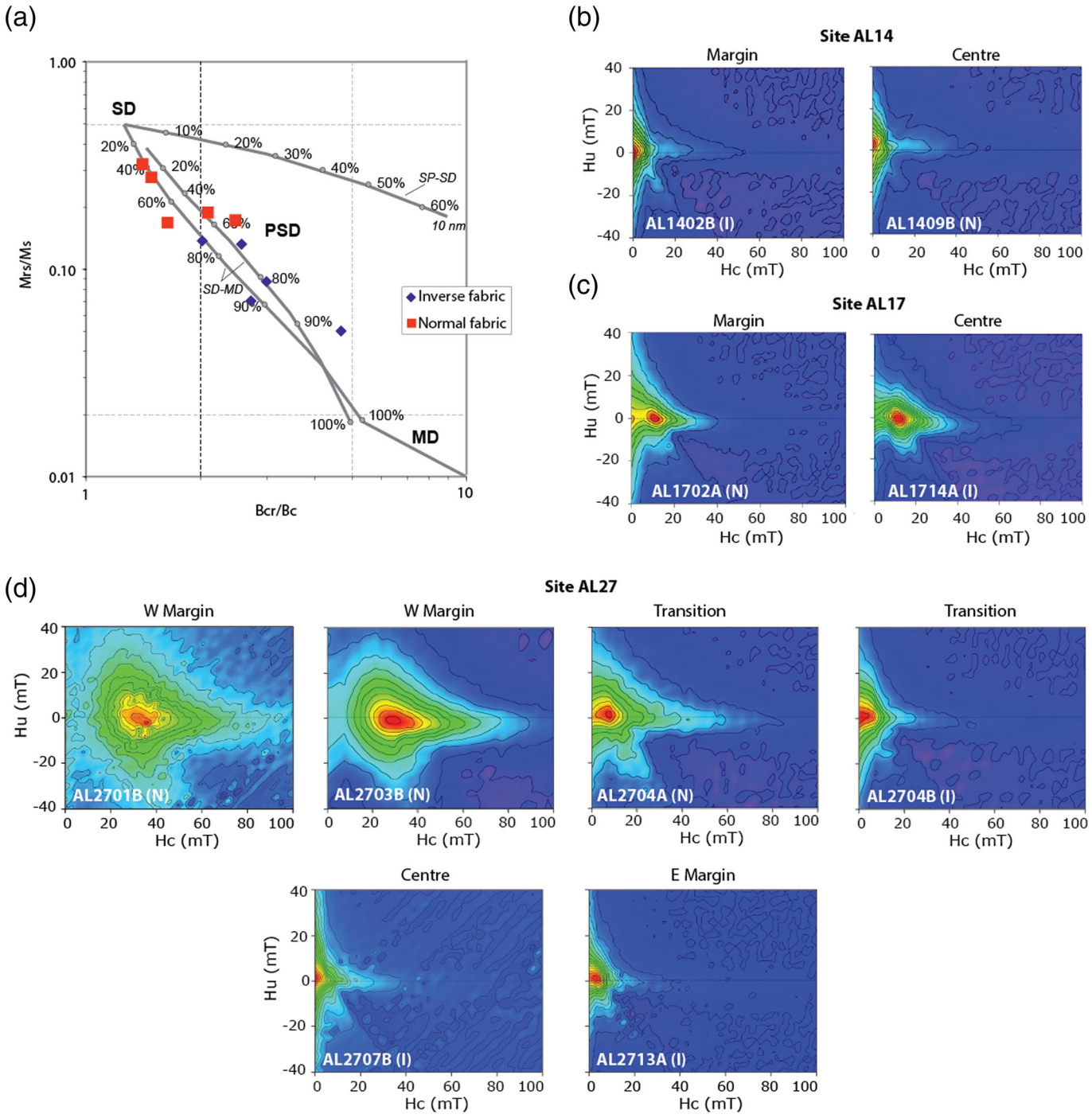

Figure 7. Hysteresis parameters, obtained at room temperature, reported on (a) bi-logarithmic Day diagrams for 10 samples from three different dikes (AL14, AL17, and AL27). We distinguished between inverse and normal fabrics by comparing them with standard percentage of MD + SD or SP + SD mixing of magnetite and titanomagnetite from Dunlop (2002). SD = single domain, PSD = pseudo-single domain, MD = multi domain, SP = super paramagnetic. FORC diagrams at room temperature for samples from sites (b) AL14, (c) AL17, and (d) AL27 characterized by normal (N) or inverse (I) fabric. The FORC diagrams are obtained on the basis of 140 curves interpreted using FORCinel software (Harrison & Feinberg, 2008) and a smoothing factor of 4 or 5. Hc = coercitivity; Hu = magnetic minerals interaction depending on the applied field.

features, while AL1714A (inverse) has PSD characteristics, with the coercivity distribution centered around 18 mT (Figure 7c).

The cores from dike AL27 show different behaviors. Samples closer to the western margin (samples AL2701B and AL2703B) show a typical single domain diagram (Figure 7d), with closed contours

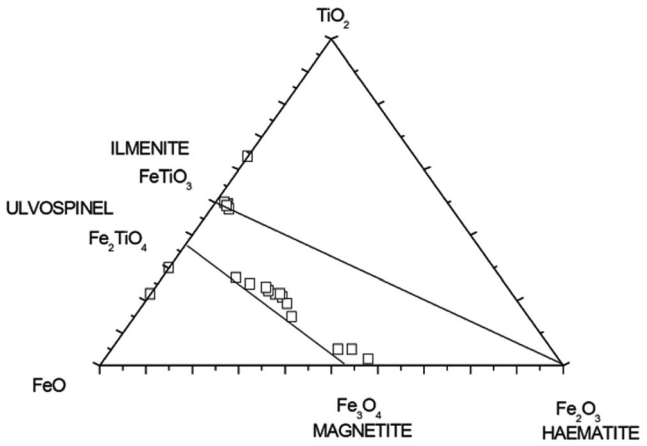

Figure 8. Composition of Fe-oxides measured by using a SEM. The data are plotted on a ternary diagram for the Magnetite-Ulvöspinel and Hematite-Ilmenite solutions. All the measurements taken on the acicular crystals correspond to Ilmenite.

centered at about 30 mT and extending to relatively high coercivity values, indicating the presence of oxidized/acicular magnetite.

The two samples from the "transition" zone show slightly different diagrams, even though belonging to the same core (AL2704). The specimen AL2704A shows feeble PSD features centered at around 10 mT and extending up to about 60 mT, while the FROC distribution of specimen 04B is peaked at the origin and extends only to about 25 mT, representing low coercivity MD grains. The diagrams of samples AL2707B and AL2713A, from the central part and eastern margin of the dike, respectively, show MD features. Therefore, FORC diagrams for site AL27 possibly show a magnetic grain size increase from the western and well-preserved dike margin toward the center and the eroded eastern margin.

Overall, the observations from FORC diagram indicate that the domain state of magnetic minerals is mainly PSD, or a combination of SD and MD, considering that the discrimination between PSD and a mixture of SD and MD is not straightforward with this kind of diagrams (Roberts et al., 2000).

For eight out of 10 samples, FORC measurements were repeated after heating the samples at different temperatures, up to 580°C. The results (Figures S5 and S6) show that, for six samples, a possible decrease in the magnetic grain size occurred due to heating (from PSD or MD at 20°C to SD at 580°C). Samples AL2707B and AL1714A show the most evident changes, moving from MD or PSD toward the SD region in the Day plots (Figures S5b and S6c).

In summary, the results of magnetic analysis (Table S1) show that the magnetic fabric is linked to the coexistence of titanomagnetite solid solutions with different percentages of Ti. The samples generally show a mixture of different proportions of MD and SD grains, with the exception of the western margin of dike AL27 (normal fabric) which shows typical SD features. In almost all cases, the magnetic grain size decreases after heating the sample at high temperatures.

4.3. Petro-Fabric and Image Analysis

4.3.1. Mineral Assemblage

For mineral fabric and assemblage, we investigated five dikes (AL06, AL09, AL14, AL22, and AL27) for a total of 13 thin sections (Table S1). Textures vary from aphanitic to porphyritic and from medium grained (e.g., dikes AL09, AL14, and AL27) to fine grained (e.g., dike AL22), even if the dikes show an overall similar composition (Trippanera et al., 2020). The main mineral phases are plagioclase (An61-51Ab39-49 and minor albite), clinopyroxene (Wo34En48Fs19-Wo27En38Fs35) and Fe-Ti oxides. Minor iron-rich olivine (Fo20-Fo66), quartz, calcite, and pyrite are also present (refer to Kretz, 1983, for acronyms). Only in a few cases some glass has been found in the groundmass for the samples located close to the margins, where a prevalence of fine grain crystals is also evident.

Fe-Ti oxides are terms of the magnetite-ulvöspinel solid solution (i.e., titanomagnetite) and ilmenite (FeTiO3) crystals (Figure 8). The iron oxides minerals of the magnetite-ulvöspinel solid solution range from Ti-rich titanomagnetite with ulvöspinel component up to ca. 60% (called TM60 from hereon), to Ti-poor titanomagnetite with Ti ca. 10–15% (TM10) (Figure 8).

The different Fe-Ti oxides can be easily recognized in the SEM images from their different shape: ilmenite crystals have a prismatic or acicular morphology, whereas magnetite-ulvöspinel crystals have a idiomorphic cubic or anhedral morphology and are usually associated with clinopyroxene (Figure 9). While crystals of magnetite-ulvöspinel series are present in all thin sections (Figure 9), the frequency of ilmenite acicular crystals is higher in samples located closer to the dike margins where the cooling rate is faster (e.g., AL1402A and AL2703A) with the exception of sample AL2204A (Figures 9e, 9f, and 9g), located in the dike center (Figure 3e). However, this sample has a very fine-grained texture compared to the previous dikes and contains some glass as groundmass (Figure 9c) possibly related to relatively rapid cooling.

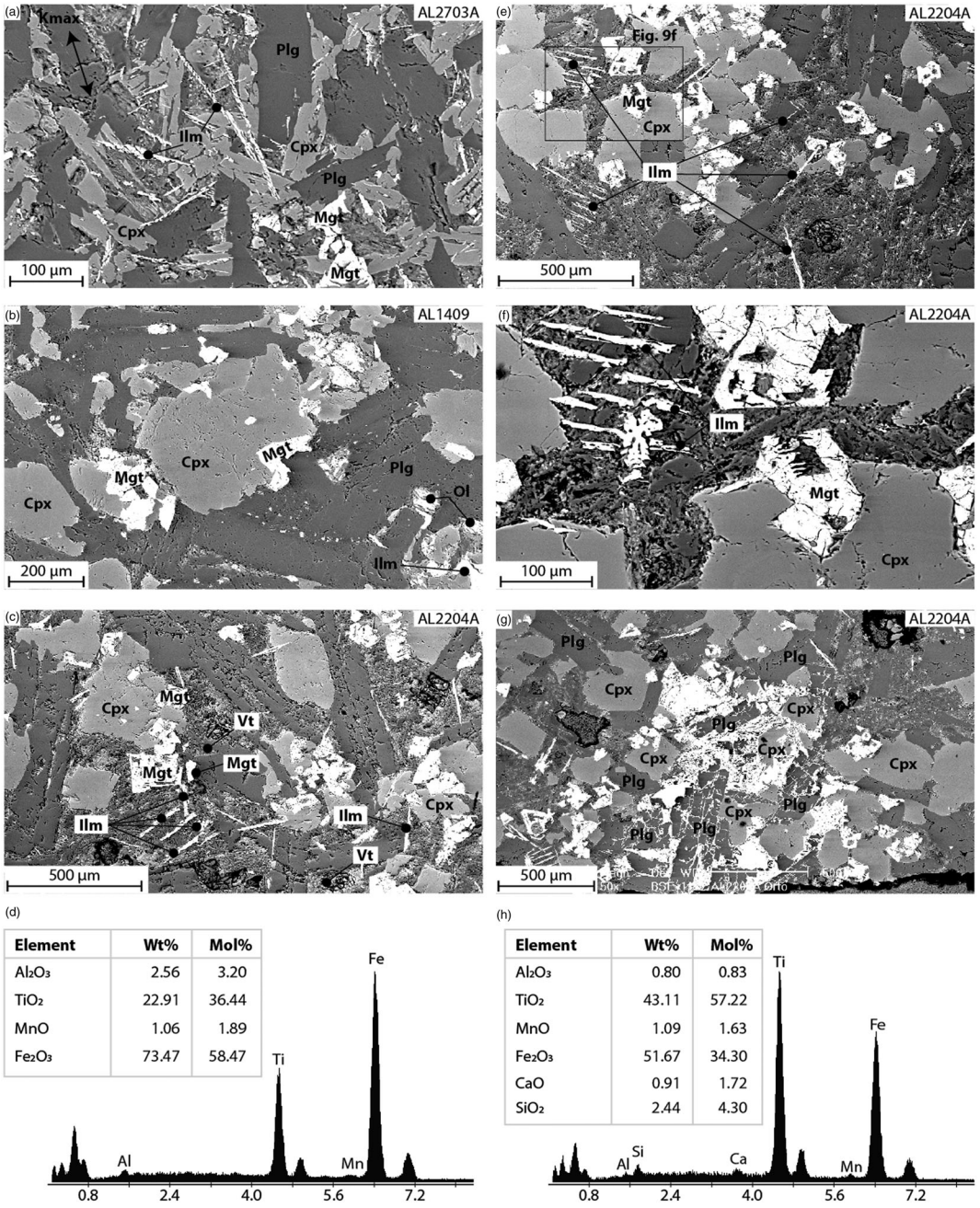

Figure 9. SEM images from thin sections on samples: (a) AL2703A (normal fabric, close to the western margin), (b) AL1409 (inverse fabric from the dike center), (c, e, f, and g) AL2204A (inverse fabric from the dike center). Plagioclase crystals (Plg) are dark gray color, Clinopyroxene crystals (Cpx) are light gray color, white coarse grains are titano-magnetite (Mgt), white acicular crystals are Ilmenite (Ilm). Some of the minerals are labeled in the figure as an example. Characteristic spectrum and tables indicating the amount in weight (Wt%) and mole (Mol%) percentage of different chemical components in (d) a titanomagnetite and (h) an Ilmenite crystal.

In general, the dikes textural association suggests that magma started crystallizing clinopyroxene and successively plagioclase and, during the last stages, titanomagnetite and ilmenite (e.g., Figure 9). With regard to the magnetite-ulvöspinel solid solution grains, they crystallized as low-Ti and high-Ti members in function of the cooling rate, as also observed in experimental studies (e.g., Mollo et al., 2013, and references

therein). All dikes show evidence of weathering with both chemical alteration (altered plagioclase, formation of chlorite, mica, etc.) and pervasive fracturing intruded by pyrite fluid (e.g., Figure 9g).

4.3.2. Image Analysis

We cut thin sections along the kmax-kmin plane to infer the orientation of crystals in four selected samples belonging to three dikes (one sample from dike AL22 and two samples from dikes AL14 and AL27). The SEM images allowed us to isolate and identify the shape and size of all the magnetic crystals (both with high and low Ti content). In particular, the crystal shape has been approximated to an ellipse enclosing the crystal itself by using the ImageJ software (Schindelin et al., 2015; https://imagej.nih.gov/ij/index.html). We identified the major and minor axes of the ellipses and then calculated the orientation of the major axis (see supporting information for further information about the method) and the roundness of each crystal (minor axis/major axis of the ellipse). Here we present the statistics of the two most representative cases belonging to the site AL27. The roundness value is mostly focused between 0.4 and 0.7 in samples where there are no or very few acicular crystals (e.g., samples AL2704B and AL1409A). On the contrary, a peak from 0.1 to 0.2 has been observed when the sample is rich in acicular or elongated crystals (e.g., samples 2703A in Figures 9a and 10a and AL2204A in Figure 9e). Overall, the orientation of the magnetic minerals (ellipse major axis enclosing the crystal) is widely distributed (Figures 10c and 10d). However, if we select only elongated crystals (roundness value <0.25) that are mostly composed by ilmenite crystals, despite some scatter, their orientation focuses on two or three preferred stretching directions, often perpendicular one to the other (e.g., samples AL2703A in Figure 10c and AL2204A in Figure 9e). The magnetic axes kmax and kmin deviate on average 18° ± 10° from the directions of the acicular and elongated crystals, but they overall fall within the range of variability of crystals directions (Figure 10c).

The size of the Fe-bearing magnetic crystals has been taken by considering the maximum and minimum axis of the ellipses enclosing each crystal. We measured five samples from four different sites (AL09, AL14, AL22, and AL27) for a total of 28 images at different scales. Overall most of the grains are smaller than 50 μm with maximum dimensions up to 200 μm (with a few exceptions above this size). Below 50 μm, grains mostly focus around 5 to 30 μm (Figure S7). The smaller grain size we are able to observe with SEM images is around 2 μm.

Optical thin section analysis is suitable to understand the distribution of nonopaque minerals, mostly plagioclase. Despite six out of seven sections parallel to the kmax show well defined nonopaque crystals, only one sample displays a preferred orientation of plagioclase (AL2703A in Figure 10a, see also Urbani et al., 2015). In this case, the preferred orientation of the crystals deviates ~30° from kmax.

4.4. Fracture Pattern

In all the investigated sites, we found at least two sets of fractures orthogonal to each other: one set subparallel to the dike margins and one almost orthogonal (a picture of each sampling site is provided in the data set by Trippanera et al., 2020). Here we report the example of four sites (AL07-08-09-10) belonging to the same dike but showing a consistent orientation of the fractures (Figure 11a), and the site AL27 in Figure S8. In particular, site AL10 shows large and continuous subvertical dike parallel fractures spaced ~1 up to ~2 m and cutting the dike along its entire length (Figures 11a and 11b). In some places also a chilled margin can be observed between the fractures. In most of the other sites the dike parallel fractures are less prominent and shorter (Figure S8). The orthogonal set contains fractures that may or may not affect the entire cross-section of the dike (Figures 11c, S8a, and S8b). These fractures show different dip, being from subvertical to subhorizontal, also intersecting each other and forming basaltic columns that are oriented horizontally and therefore perpendicularly to the dike margins (e.g., Figures 11d, 11e, S8a, and S8c).

5. Discussion

5.1. Origin of Magnetic Fabric in Alftafjordur Dikes

The origin of the geometrically inverse AMS fabric is one of the main controversial topics of the AMS studies, as it can lead to erroneous interpretations when used for reconstructing magma flow direction (e.g., Almqvist et al., 2012; Rochette et al., 1999). The occurrence of such anomalous AMS fabrics, mainly in basaltic dikes, has been attributed to different origins, as related to the magnetic mineralogy with the prevalence of SD grains (Potter & Stephenson, 1988), complex magmatic and tectonic processes during or after the dike emplacement (Khan, 1962; Rochette et al., 1999) or a combination of the two.

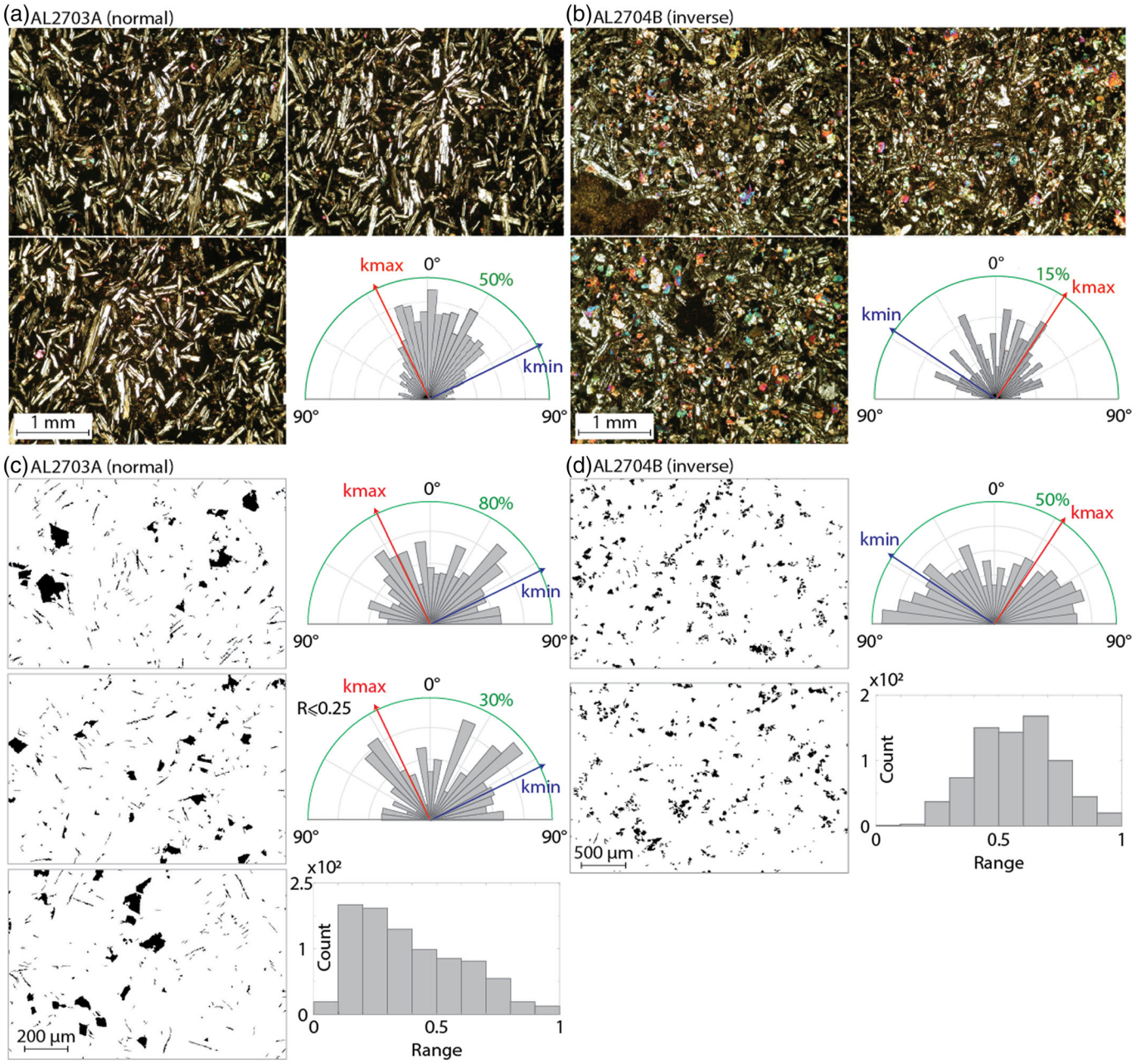

Figure 10. Image analysis on two thin sections of site AL27. Thin sections have been cut along the plane containing kmax and kmin. Optical microscope images from thin sections and rose diagrams showing the orientation of the plagioclases in samples (a) AL2703A and (b) AL2704B. Extracted shapes of Fe-oxides (black) from SEM microscope images, rose diagram, and histogram showing the orientation and the roundness (R) of the Fe-oxides for samples (c) AL2703A and (d) AL2704B. Roundness is equal to 1 for a circle. For the sample AL2703A we also separately plotted the orientation of elongated crystals ($R \leq 0.25$), mostly ilmenite. Within the rose diagrams we plotted the orientation of the maximum (kmax) and minimum (kmin) magnetic axis obtained by AMS measurements at H = 300 A/m. The radius of each semicircle corresponds to the frequency indicated in green.

The Alftafjordur dike swarm represents a typical case for further studying the origin of anomalous (i.e., inverse and mixed) magnetic fabrics in basaltic dikes. The low field (H = 300 A/m) AMS measurements on the Alftafjordur dikes, in fact revealed that most of the dikes (80% of samples, Figure 2) show a clear and well-clustered geometrically inverse AMS fabric (kmax subperpendicular to the dike margin) with a relatively high value of the anisotropy degree (Pj). In some cases, we also observe a mixed AMS fabric (*sensu* Kissel et al., 2010), characterized by the coexistence of inverse and normal (kmax is subparallel to the dike margin) AMS fabric across the same dike (see dike AL27 and AL14 in Figure 4). In one specific case (site

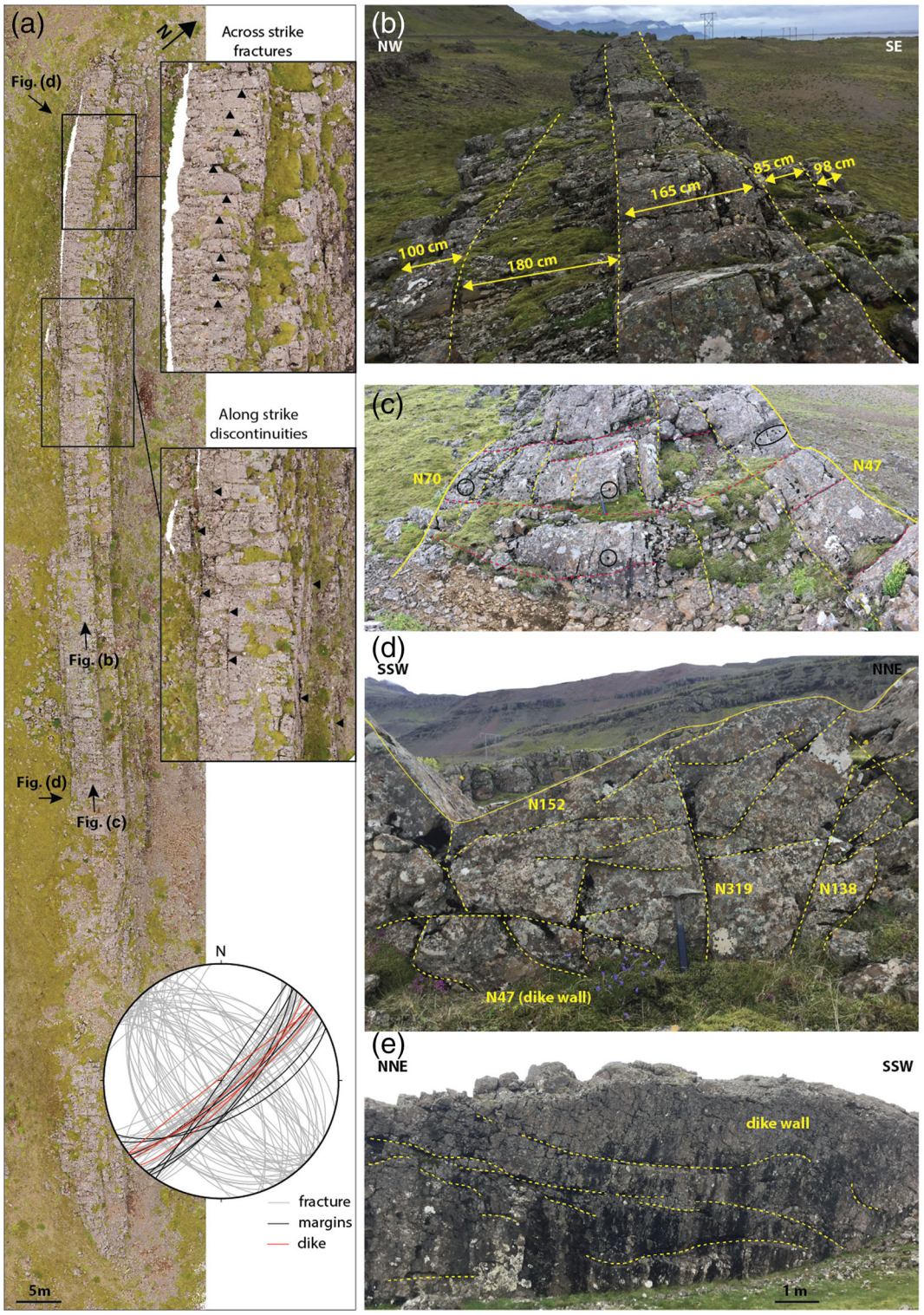

Figure 11. Fracture pattern within dikes. (a) Orthomosaic obtained by a drone survey at site AL10 and stereonet showing fracture and margins orientations measured at sites AL07-08-09-10 (same dike). In the insets triangles point to major across and along strike discontinuities. Picture of (b) the dike top, (c) the sampling site (black circles show the coring location), (d, e) the dike margin. Some of the major fractures and discontinuities are also highlighted with a dashed line. Picture location is indicated in Figure 11a.

AL27) we observe normal AMS fabric in samples close to the dike margin (e.g., samples AL2701 to AL2703, Figures 3 and 4) with a progressive switch to inverse AMS fabric toward to the dike center (Figure 5; Urbani et al., 2015).

The multidisciplinary approach (magnetic, petrographic, and field analyses) proposed in this work allows us to understand the possible origin of the widespread occurrence of inverse AMS fabrics. We first evaluate the occurrence of the main magnetic carriers (i.e., ferromagnetic minerals) and their magnetic grain size; successively we discuss also the contribution and the distribution of other paramagnetic minerals (i.e., ilmenite and silicate minerals).

The results of the k-T curves (Figure 6) and SEM analysis (Figures 8 and 9) suggest that the dikes are characterized by a complex mixture of different magnetic carriers. Rock magnetic and SEM analyses indicate that titanomagnetites with variable content of Ti are present in the samples, as commonly found in similar mafic dikes of Iceland (Craddock et al., 2008; Eriksson et al., 2014; Kissel et al., 2010) or other dike swarms (Borradaile & Gauthier, 2001; Raposo & Ernesto, 1995). These titanomagnetites, that have a size variable from 2 to 200 μm from SEM analysis, coexist with other Fe-Ti oxides such as acicular and elongated ilmenite ($FeTiO_3$) crystals.

The hysteresis parameters and FORC diagrams indicate that the inverse fabric samples are characterized by prevailing PSD and MD features; in contrast, a few samples with normal fabric show a SD behavior. These results indicate that the occurrence of geometrically inverse AMS fabric in the sampled dikes cannot be explained with the presence of SD grains.

Another aspect to be tested for revealing the origin of the prevalent inverse fabric, when the AMS is measured at low-field, is to decipher the contributions of the different magnetic carriers to the measured AMS. For example, Kissel et al. (2010) observed a fabric variation from inverse to normal upon heating within dikes showing a mixed fabric. The authors interpret this variation due to the oxyexsolution of larger magnetite grains with high-Ti content and the formation of smaller low-Ti magnetite and ilmenite lamellae with a magnetic axis parallel to the dike margins. To test this, we performed AMS measurements of selected samples varying both the temperature (from ambient temperature to 580°C) and the applied magnetic field (200 and 600 A/m; Chadima et al., 2009). Differently from Kissel et al. (2010) and with the exception of a few samples, we do not observe any systematic variation of the magnetic axis orientation with various magnetic fields or temperatures (Figures 5 and S2). The same behavior is also observed with the AARM analysis (Figure S3), suggesting that the influence of the paramagnetic minerals (e.g., silicate matrix and ilmenite) in our AMS analysis is negligible and the AMS is mainly representative of ferromagnetic minerals. This is consistent with the high mean value of the bulk magnetic susceptibility k (e.g., Cañón-Tapia, 2004, and references therein) and magnetic anisotropy degree Pj in all the inverse fabric samples (Table 1 and Figure 2b).

Moreover, SEM analysis on thin sections parallel to the kmax direction revealed that the acicular ilmenite crystals occur mostly in normal (AL2703A) and, less frequently, in inverse fabric (AL2204A) samples. In addition, when present, ilmenite grains can be either parallel or perpendicular to the maximum susceptibility axis (Figure 10c) in the same specimen. This variable orientation would have scattered the magnetic axis orientation, whereas AMS results show that kmax and kmin are usually very well grouped in all sites (Figure S1 and database by Trippanera et al., 2020). We conclude that even though ilmenite crystals may have a minor influence on the magnetic fabric, they are not the main cause of the systematic inverse fabric found in all the dikes.

Contrary to ilmenite, titanomagnetite grains with variable Ti-content were observed in all thin sections (Figure 10b). Titanomagnetites do not apparently show any systematic elongation or preferred orientation and are often associated with clinopyroxene grains (Figures 9e–9g) testifying a coeval growth during cooling. Recent experimental studies (e.g., Mollo et al., 2011, 2013) demonstrated that a coarse-grained subeuhedral shape titanomagnetite is indicative of a relatively low cooling rate (0.5°C/min, Mollo et al., 2013), as expected for the central part of the dike. The analysis of the distribution of plagioclase crystals (having an elongated shape) in thin sections shows that they are rarely iso-oriented. Therefore, this is an additional reason to exclude that plagioclase network (paramagnetic), which formed during the early phases of crystallization (cf. Mattsson et al., 2011), may influence the AMS. However, we found a good example of

plagioclase iso-orientation from the margin of the site AL27 (sample AL2703A), where the crystals are almost subparallel to kmax (Figure 10a). From the three cores at the margin of dike AL27 a well-defined normal fabric has been identified by using the AMS analysis and the presence of SD grains has been revealed in two samples (Figure 7b), potentially leading to a misinterpretation of the reason of magnetic axis orientation. In this case, the plagioclase orientation is useful to confirm that the magnetic fabric in the margin of AL27 dike is a reliable indicator of the magma flow during the dike emplacement (Urbani et al., 2015). Contrary to classical expectations (e.g., Chadima et al., 2009), this dike shows a general magnetic grain size increase from the margin (SD domain) to the dike center (MD to PSD domain), that oppositely correlates with the AMS fabric, changing from normal at the margin to inverse at the dike center (Figure 7). This change in the magnetic and physical properties of rocks also corresponds to a major discontinuity along the dike (Figures 4a and S8) between a strongly foliated fabric, parallel to the dike margin, and a visually homogeneous rock with subhorizontal cooling joints oriented orthogonally to the dike margins.

In summary, the insignificant presence of SD particles in inverse AMS samples, the overall high value of the anisotropy degree, the scarce iso-orientation of both plagioclase and ilmenite along with the fact that ilmenite crystals are not present in all samples suggest that the main magnetic carrier is PSD or SD + MD titanomagnetite, which is ubiquitous throughout the dikes. The mineralogical compositional data together with the results of thermomagnetic curves and the field dependence of magnetic susceptibility further confirm that the titanomagnetites are characterized by a variable Ti-content ($0.1 < x < 0.6$, $Fe_{3-x}Ti_xO_4$).

5.2. Implications on the History of Exhumed Dikes

Our AMS results are consistent with those obtained along the same dike swarm (Eriksson et al., 2014) and from the Reydarfjordur dike swarm to the north of Alftafjordur (Kissel et al., 2010), where an anomalous AMS fabric or a prevalence of inverse AMS fabrics has been also observed. According to Kissel et al. (2010) both normal and inverse AMS fabric are primary fabrics carried by titanomagnetite grains, reflecting different physico-chemical conditions during the emplacement of the magma. Also, in the Alftafjordur dike swarm, the main magnetic carriers are titanomagnetites but, differently from Kissel et al. (2010), we do not observe any clear change in the physico-chemical properties of the titanomagnetite across the dikes.

Eriksson et al. (2014) interpreted the anomalous AMS fabric as the effect of tectonic shear during magma emplacement based on the agreement between the fracture pattern at the margins of the dikes and the shear stress affecting the area during the rift evolution. However, their observations focused on selected dikes with kmax parallel to the dike margins, whereas the majority of our measurements show well clustered kmax subperpendicular to the dike margins. Moreover, besides the fractures on the host rocks close to the dike margins, our analysis highlights that dikes are also strongly affected by a pervasive fracturation over their entire width and length.

Another aspect to take into account is the possibility that the flow within a dike can be turbulent or transitional to a laminar regime for pressure values greater than 10 MPa, corresponding to a depth higher than 300 m (Lanzafame et al., 2017). These emplacement conditions could apply to the Alftafjordur dike swarm, since the actual surface, where the sampling has been carried out, corresponds to a paleodepth of 1 to 1.5 km (e.g., Walker, 1974), where the pressure could have reached more than 20 MPa (Lanzafame et al., 2017). It may also happen that at the dike margins, due to the higher friction and faster cooling, the flow slows down creating the conditions for a locally laminar flow while the dike center is still under turbulent or nonlaminar conditions. Additionally, turbulence or nonlaminar flow conditions may also be created by several other local factors, such as magma propagation within irregular fractures (Gudmundsson, 1983; Kissel et al., 2010), stiffness contrasts in the country rocks (e.g., Geshi et al., 2012; Gudmundsson, 2002; Gudmundsson & Loetveit, 2005; Gudmundsson & Philipp, 2006), and compositional zonation (Eriksson et al., 2011; Hrouda et al., 2019). Even though the latter phenomena may affect the orientation of the magnetic crystals and therefore the overall AMS results, we can exclude any influence of peculiar local dike conditions thanks to the sampling strategy: in the sampling sites the dikes do not show any of above-mentioned conditions. Moreover, the consistency of AMS results, showing inverse fabric in the same dike sampled in different locations (e.g., sites AL07-08-09-10), and even more the fact that the entire dike swarm shows the same magnetic principal axes behavior, strongly suggests that the inverse fabric cannot be related to random local conditions within the dike or in the host rocks. Moreover, for a nonlaminar flow, we would expect a scatter on the magnetic axis orientations. A nonlaminar flow, on one hand, could explain the lack of

iso-orientation of the plagioclase in almost all the samples (e.g., Figure 10b), but on the other hand, it would be in contrast with the well clustered magnetic axes shown by our AMS data. We therefore suggest that the flow conditions within the dike are not the primary cause of the inverse fabric.

An additional issue is the possible occurrence of composite fabric due to metasomatism processes (Silva et al., 2008) or different crystallization timing of the mineral assemblage (Silva et al., 2014). In these cases, the paramagnetic mineral orientations may reflect the primary magma flow in the dike, whereas the orientation of magnetic minerals in the matrix is affected by the late stage of cooling. However, field observations on the whole dike swarms of Eastern Iceland (e.g., Eriksson et al., 2011, 2014; Kissel et al., 2010; Paquet et al., 2007; Urbani et al., 2015; this study) along with our thin sections' analysis do not highlight any diffuse metasomatism process affecting the dike swarms. Moreover, the composite fabric is associated with a reduced grain size due to the exsolution of magnetic minerals. This promotes the presence of SD magnetic grains associated with the inverse fabric (Silva et al., 2008). In our dikes where AMS analyses show inverse fabric, we did not observe a predominant presence of SD grains or typical oxidation-exsolution textures associated with oxidation/metasomatic processes nor the presence of massive secondary minerals assemblage (like chlorite, sphene, and calcite). Additionally, in thin sections, we did not observe any noncoaxial ferromagnetic and paramagnetic fabric (e.g., Silva et al., 2014) potentially highlighting a composite fabric. If this would have happened, paramagnetic minerals (e.g., plagioclase) should have been aligned according to the primary flow. On the contrary, magnetic minerals should have a different orientation, reflecting the secondary and later stage of dike cooling. This can be possible only at the side of the dike AL27, where we observed a combination of preferred orientation of the paramagnetic minerals and SD magnetic grains. This may suggest that the smaller magnetic grains in the matrix are orthogonal to the dike wall, whereas the plagioclase crystals (paramagnetic) are parallel to it, in agreement with a possible primary magma flow. This may explain why we surprisingly observed SD grains in a normal fabric setting. Finally, if noncoaxial fabric occurs between the phenocrysts and the matrix, we cannot investigate it since the matrix grain size would be smaller than the microscope resolution (0.2 μm).

Our field analysis highlighted that the fracture pattern of all dikes is characterized by at least two sets of major fractures: one set subparallel to the dike margins and one almost orthogonal to them. The orthogonal fractures define basaltic columns oriented horizontally and perpendicularly to the dike margins (e.g., Figures 11 and S8; Ellwood, 1979). This suggests that, similarly to the columnar basalts, the formation of the orthogonal fracture pattern is primarily due to the dike cooling, whereas the dike parallel fractures could be also related to different velocities of the magma flow (especially close to the dike margins) or by multiple phases of magma intrusion (subparallel one to the other) along the same path or tectonic shear planes (Eriksson et al., 2014). Additional effects of the tectonic strain and successive weathering of the exposed rocks could also have contributed to this extensive fracture formation.

Interestingly, comparing the directions of kmax and kmin with the orientation of the fracture sets within the dikes, we found that the magnetic principal axes may be parallel to at least one of the sets (Figure 12). In particular, where the magnetic fabric is normal (e.g., site AL16), kmax is parallel to the subvertical fractures (i.e., parallel to the dike orientation), but in dikes showing an inverse fabric, kmax is parallel to the fractures trend which is orthogonal to the dike margins (e.g., sites AL07, 08, 09, 10, and AL28) and therefore parallel to the long axis of the columns (Figure 12). This is similar to what was observed in the columnar basaltic lava, where the long magnetic axis is subvertically oriented and parallel to the long axis of the columns, possibly in response to the cooling joint formation and to the induced internal flow within the column during the late cooling stage (Almqvist et al., 2012; Hrouda et al., 2015; Mattsson et al., 2011).

We propose a different model for the response of the magnetic fabric for dikes emplaced close to the surface and those which cooled at depth. When a dike is close to the surface the cooling can be very fast, allowing the magma to rapidly "freeze," while the magma overpressure is driving the magma upward. Therefore, it is likely that the magnetic minerals would be imbricated according to the magmatic flow directions and that, consequently, the AMS fabric would reflect the real flow direction through the whole thickness of the dike. In this case, kmax is parallel to the main flow and to dike margins (Figure 13a). In contrast, at higher depth in the subsurface (depth >1 km), the cooling history could be completely different and characterized by more complex cooling rate gradient and viscosity (see also Silva et al., 2010). In particular, the cooling rate of deep dikes can be faster close to the margin and slower in the dike center, especially if the dike thickness is

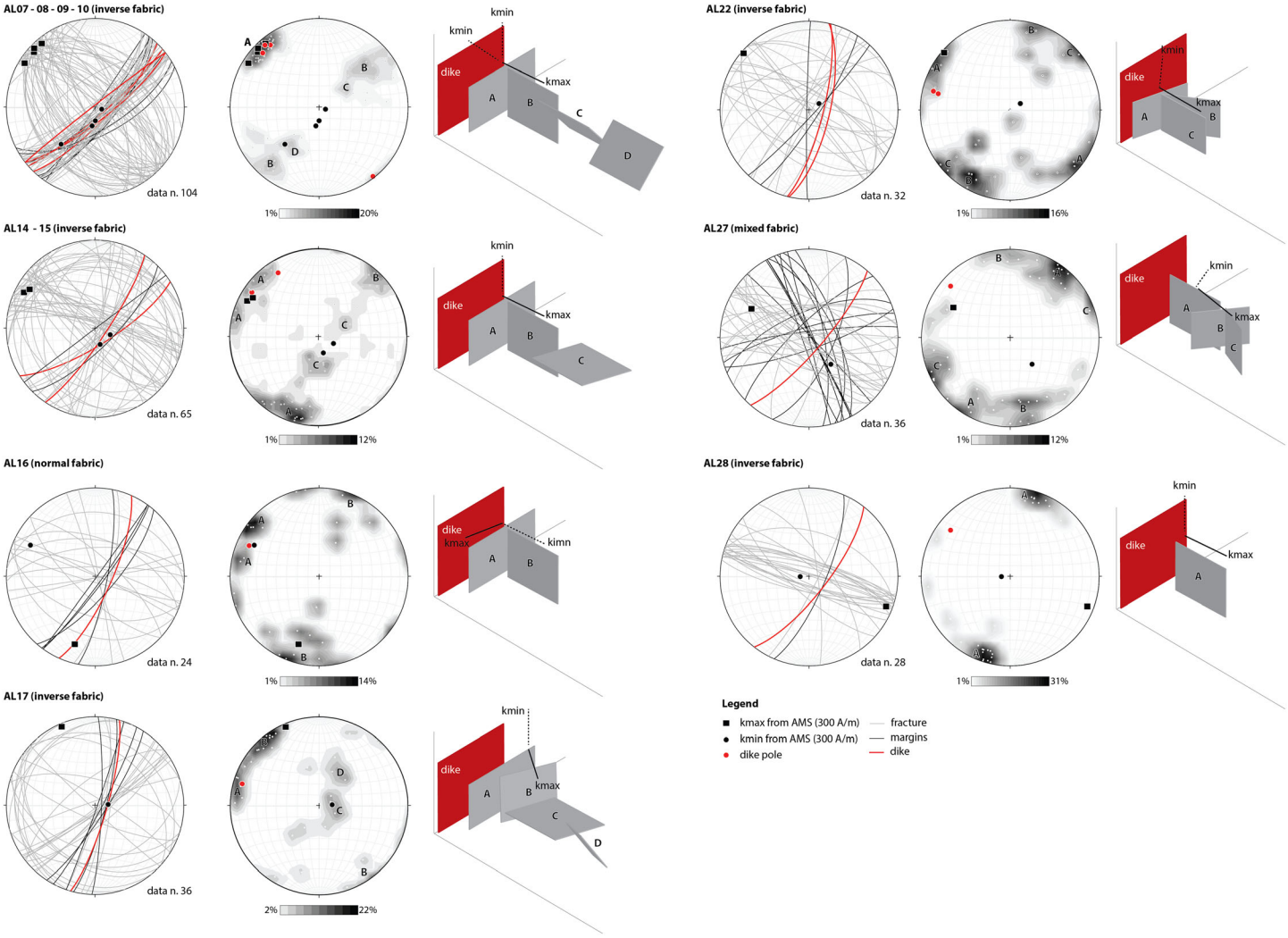

Figure 12. Comparison between the fracture pattern measured in the field and the magnetic axes obtained by AMS measurements with H = 300 A/m for 11 sites. Data from sites AL07-08-09-10 and AL14-15 are plotted together since they belong to the same dike. (Left column) Stereonets showing the orientation of the dike, of the fractures and of the magnetic axis. (Central column) Densities of the fractures' poles (see caption of Figure 2 for the method) compared to the dike pole and the magnetic axes orientation. Each letter indicates a set of fractures. (Right column) 3-D schematic view showing the geometric relationships among the dike margin (red), each set of fracture (gray) and the magnetic axes (black solid and dashed lines).

quite large, as for the Iceland dike swarms (e.g., Urbani et al., 2015). These conditions allow the development of dike-orthogonal cooling joints propagating from the margin to the inner portion of the dike, in a similar manner to the columnar joints on thick lava flows (Figure 13a). We suggest that, similarly to what happens in the columnar joint case (Almqvist et al., 2012; Mattsson et al., 2011), the joints' propagation and the progressive slower cooling may generate a secondary magma migration during the cooling stage of deep dikes. This late magmatic adjustment can drive the late crystallization and the preferred alignment of coarse grained titanomagnetites (Figure 13b). In this case, the magnetic crystals will be oriented parallel to the long axis of the column (therefore perpendicularly to the dike margins), and AMS shows a systematic inverse geometric fabric all over the dike length (Figure 13). If the margin of the dike is affected by fast cooling and high shear the normal geometric fabric may be preserved (Figure 13a).

Moreover, within dikes cooled at subsurface, when the magmatic pressure (directed upward) decreases and the cooling phase begins, the weight of the overburden solidifying magma may induce an additional lithostatic stress downward directed and linearly increasing with depth. This stress, perpendicularly oriented to the secondary flow, may also enhance the subhorizontal and dike-orthogonal melt migration that along

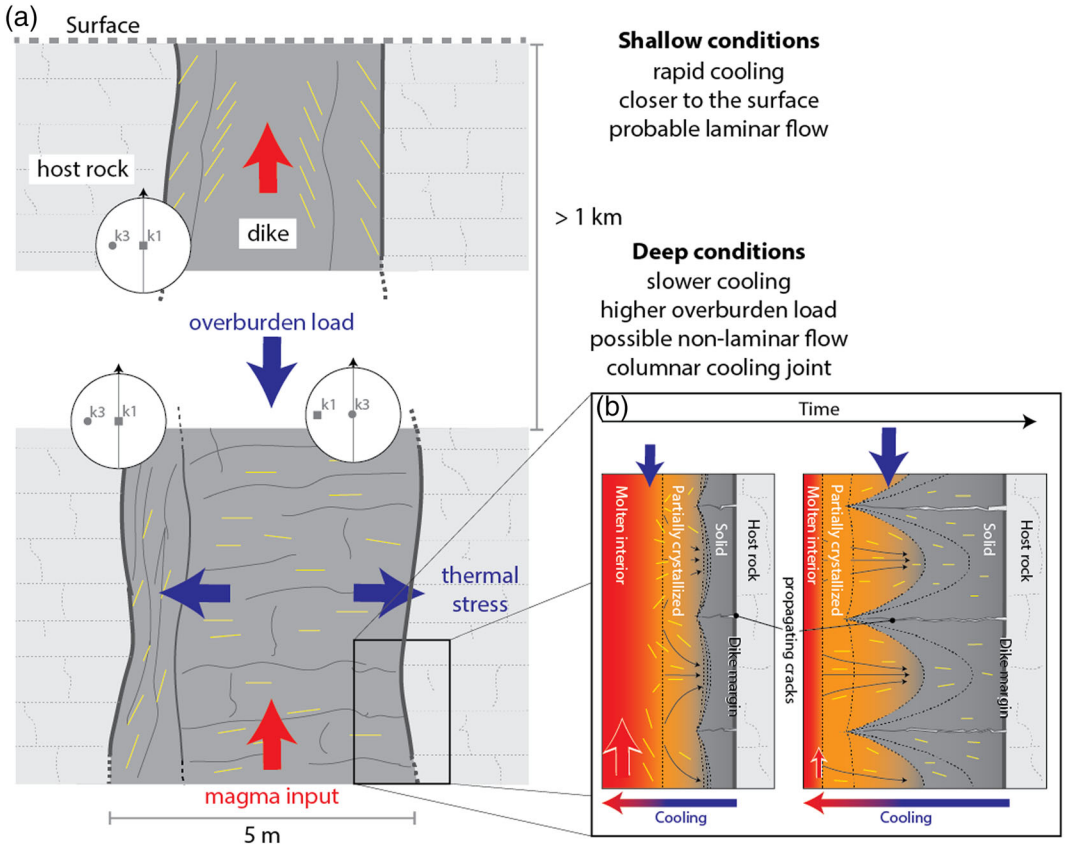

Figure 13. (a) Schematic illustration of the geometric magnetic fabric in a dike close to the surface and at depth > 1 km. Close to the surface, where a rapid cooling occurs the magnetic minerals (yellow lines) reflect the flow within the dike and AMS show an overall normal geometric fabric (the circle represents the schema of the AMS result). At depth, the cooling rate is slower and subhorizontal cooling joints develop, leading to a geometric inverse AMS fabric. Occasionally the magnetic minerals can reflect the flow direction at the dike margins where the shear and the cooling rate are higher. Vertical dimension is not to scale. (b) Illustration of progressive cooling and relative isotherms during the formation of subhorizontal cooling joints in a deep dike (after Mattsson et al., 2011). The crack propagation into the dike increases the steepness of the isotherms affecting the orientation of the magnetite crystals. Blue and red arrows indicate the overburden load and magma input respectively.

with cooling joints development helps to constrain the orientation and alignment of coarser grained titanomagnetites, forming at lower cooling rates (Mollo et al., 2013).

The coexistence of dike parallel and dike orthogonal or oblique fractures can also explain the occurrence of normal and inverse AMS fabric within the same dike (as for example at sites AL14 and AL17) without observing any consistent mineral phase change or prevalence of SD grains (Figure 7a).

Overall, in this work we demonstrated that the interpretation of the magnetic fabric is not always straightforward and can be even trickier for an old and extensive dike swarm such as those cropping out in Eastern Iceland. Despite several authors attempted to interpret the flow directions in Eastern Iceland ending up with a vertical or oblique propagation of the flow, the full understanding of the emplacement process and magma flow direction always required additional data to the low-field AMS analysis. Indeed, a simple low-field AMS analysis can be misleading, and additional observations from the macroscale (fracture at the outcrop scale) to the microscale (e.g., thin section analysis) are usually needed for old and exhumed dike swarms.

6. Conclusions

In this work we performed AMS analysis on 19 dikes belonging to the fissure swarm of the Alftafjourdur volcanic system (in Eastern Iceland), and then we investigated the origin of the geometrically inverse magnetic fabric by using a multiscale and multidisciplinary approach. We obtained the following:

1. Low field AMS measurements (H = 300 A/m) show a geometrically inverse magnetic fabric (kmax perpendicular to the dike margins) in almost all dikes (80% out of 383 samples). This fabric is also consistent with AMS measurements on selected cores performed at different magnetic fields (H = 200 and 600 A/m) and after heating (up to 580°C), suggesting that the data were not influenced by the coexistence of different mineralogic phases.
2. Hysteresis parameters, FORC and AARM measurements exclude the prevailing occurrence of SD grains in inverse samples, suggesting that they are not the carriers of the inverse AMS fabric. We found prevailing SD grains in only two samples, located at the dike margin, but showing a normal AMS fabric. However, in this margin, the magnetic fabric is also consistent with the well-organized orientation of the plagioclase minerals.
3. Thermomagnetic curves and SEM thin section analyses revealed the presence of two main types of Fe-oxides: acicular paramagnetic ilmenite (more frequent close to the margins) and ubiquitous ferrimagnetic titanomagnetite, characterized by a variable Ti-content ($0.1 < x < 0.6$). The high values of the magnetic susceptibility, along with the fact that ilmenite crystals are not iso-oriented and not present in all inverse AMS samples, suggest that the magnetic fabric is carried by titanomagnetite in a broad grain size range. Thin sections suggest a range with size of 2 to 200 μm.
4. All dikes are intensely fractured, with sets of fractures mostly orthogonal to the dike margins isolating horizontal basaltic columns formed during the cooling stage of the dike. Since kmax is parallel to this orthogonal fracture pattern, we suggest that the distribution of the coarse grain magnetite is controlled by the dike cooling stage and aligns parallel to the horizontal basaltic columns due to the weight of the overburden magma and the internal flow (relaxation phase) in the basaltic columns with a mechanism similar to the columnar basalts. This seems to be the most likely mechanism to explain the occurrence of systematic geometrically inverse magnetic fabric in the old and deep dikes in Eastern Iceland. These features (columnar joints and related inverse fabric) are more common with deeper dikes.

Data Availability Statement

The raw data about AMS and AARM analysis along with the images of all thin sections and Day Plot data are accessible in Trippanera et al. (2020) (data set repository: http://pmd.gfz-potsdam.de/panmetaworks/review/d461b042d9f9f2ce0aa768be33166caf7b3e109ca3c1a66673678b6f66c02a12/).

Acknowledgments

We would like to thank Sergio Lo Mastro (Roma Tre University) assisting us for the measurements and identification of minerals at the Electronic Microscope along with the staff of the Laboratory of Experimental Volcanology and Petrology from Roma Tre University for providing access to the optical microscope and assistance in the thin section analysis. This project has been founded by PRIN 2009 funds (2009H37M59, responsible V. Acocella) and partially by the King Abdullah University of Science and Technology (KAUST) BAS/1/1353-01-01. M. Porreca acknowledges the support of ASI (Agenzia Spaziale Italiana) under the ASI-UniPG agreement 2019-2-HH.0. S. Urbani acknowledges support from Roma Tre University MSc thesis project grant. We would like to thank the Associate Editor Mark J. Dekkers and the reviewers Pedro Silva and Fátima Martín-Hernández for the helpful comments and constructive review.

References

Allmendinger, R. W., Cardozo, N. C., & Fisher, D. (2013). *Structural geology algorithms: Vectors & tensors: Cambridge*. England: Cambridge University Press. 289 pp

Almqvist, B. S. G., Bosshard, S. A., Hirt, A. M., Mattsson, H. B., & Hetényi, G. (2012). Internal flow structures in columnar jointed basalt from Hrepphólar, Iceland: II. Magnetic anisotropy and rock magnetic properties. *Bulletin of Volcanology*, *74*(7), 1667–1681. https://doi.org/10.1007/s00445-012-0622-0

Archanjo, C. J. (2002). Fabric of the Rio Ceará–Mirim mafic dike swarm (northeastern Brazil) determined by anisotropy of magnetic susceptibility and image analysis. *Journal of Geophysical Research*, *107*(B3). https://doi.org/10.1029/2001JB000268

Bascou, J., Camps, P., & Dautria, J. M. (2005). Magnetic versus crystallographic fabrics in a basaltic lava flow. *Journal of Volcanology and Geothermal Research*, *145*(1–2), 119–135. https://doi.org/10.1016/j.jvolgeores.2005.01.007

Borradaile, G. J., & Gauthier, D. (2001). AMS-detection of inverse fabrics without AARM, in ophiolite dikes. *Geophysical Research Letters*, *28*(18), 3517–3520. https://doi.org/10.1029/2001GL012976

Callot, J. P., Geoffroy, L., Aubourg, C., Pozzi, J. P., & Mege, D. (2001). Magma flow directions of shallow dykes from the East Greenland volcanic margin inferred from magnetic fabric studies. *Tectonophysics*, *335*(3–4), 313–329. https://doi.org/10.1016/S0040-1951(01)00060-9

Cañón-Tapia, E. (2004). Anisotropy of magnetic susceptibility of lava flows and dykes: A historical account. *Geological Society Special Publication*, *238*(1988), 205–225. https://doi.org/10.1144/GSL.SP.2004.238.01.14

Cañón-tapia, E., & Chávez-Álvarez, M. J. (2004). Theoretical aspects of particle movement in flowing magma: Implications for the anisotropy of magnetic susceptibility of dykes. *Geological Society Special Publication*, *238*, 227–249. https://doi.org/10.1144/GSL.SP.2004.238.01.15

Cardozo, N., & Allmendinger, R. W. (2013). Spherical projections with OSXStereonet. *Computers & Geosciences*, *51*, 193–205. https://doi.org/10.1016/j.cageo.2012.07.021

Chadima, M., Cajz, V., & Týcová, P. (2009). On the interpretation of normal and inverse magnetic fabric in dikes: Examples from the Eger Graben, NW Bohemian Massif. *Tectonophysics*, *466*(1–2), 47–63. https://doi.org/10.1016/j.tecto.2008.09.005

Chadima, M., & Jelínek, V. (2008). Anisoft 4.2.—Anisotropy data browser. *Contributions to Geophysics and Geodesy*, *38*, 41.

Craddock, J. P., Kennedy, B. C., Cook, A. L., Pawlisch, M. S., Johnston, S. T., & Jackson, M. (2008). Anisotropy of magnetic susceptibility studies in tertiary ridge-parallel dykes (Iceland), tertiary margin-normal Aishihik dykes (Yukon), and Proterozoic Kenora-Kabetogama composite dykes (Minnesota and Ontario). *Tectonophysics*, *448*(1–4), 115–124. https://doi.org/10.1016/j.tecto.2007.11.035

Day, R., Fuller, M. D., & Schmidt, V. A. (1977). Hysteresis properties of titanomagnetites: Grain size and composition dependence. *Physics of the Earth and Planetary Interiors*, *13*, 260–266. https://doi.org/10.1016/0031-9201(77)90108-x

De Wall, H. (2000). The field-dependence of AC susceptibility in titanomagnetites: Implications for the anisotropy of magnetic susceptibility. *Geophysical Research Letters*, *27*(16), 2409–2411. https://doi.org/10.1029/2000GL008515

Dragoni, M., Lanza, R., & Tallarico, A. (1997). Magnetic anisotropy produced by magma flow: Theoretical model and experimental data from Ferrar dolerite sills (Antarctica). *Geophysical Journal International*, *128*(1), 230–240. https://doi.org/10.1111/j.1365-246X.1997.tb04083.x

Dunlop, D. J. (2002). Theory and application of the Day plot (Mrs/Ms versus Hcr/Hc) 1. Theoretical curves and tests using titanomagnetite data. *Journal of Geophysical Research*, *107*(B3), 2056. https://doi.org/10.1029/2001JB000486

Dunlop, D. J., & Özdemir, Ö. (1997). *Rock magnetism. Fundamentals and frontiers. Cambridge Studies in Magnetism Series*. xxi 573 pp. Cambridge, New York, Port Chester, Melbourne, Sydney: Cambridge University Press. ISBN 0 521 32514 5

Ellwood, B. B. (1978). Flow and emplacement direction determined for selected basaltic bodies using magnetic susceptibility anisotropy measurements. *Earth and Planetary Science Letters*, *41*, 254–264. https://doi.org/10.1016/0012-821x(78)90182-6

Ellwood, B. B. (1979). Anisotropy of magnetic susceptibility variations in Icelandic columnar basalts. *Earth and Planetary Science Letters*, *42*, 209–212. https://doi.org/10.1016/0012-821x(79)90026-8

Eriksson, P. I., Riishuus, M. S., & Elming, S. A. (2014). Magma flow and palaeo-stress deduced from magnetic fabric analysis of the Álftafjördur dyke swarm: Implications for shallow crustal magma transport in Icelandic volcanic systems. *Geological Society Special Publication*, *396*, 107–132. https://doi.org/10.1144/SP396.6

Eriksson, P. I., Riishuus, M. S., Sigmundsson, F., & Elming, S. Å. (2011). Magma flow directions inferred from field evidence and magnetic fabric studies of the Streitishvarf composite dike in East Iceland. *Journal of Volcanology and Geothermal Research*, *206*(1–2), 30–45. https://doi.org/10.1016/j.jvolgeores.2011.05.009

Ferré, E. C. (2002). Theoretical models of intermediate and inverse AMS fabrics. *Geophysical Research Letters*, *29*(7), 311–314. https://doi.org/10.1029/2001GL014367

Geoffroy, L., Callot, J. P., Aubourg, C., & Moreira, M. (2002). Magnetic and plagioclase linear fabric discrepancy in dykes: A new way to define the flow vector using magnetic foliation. *Terra Nova*, *14*, 183–190. https://doi.org/10.1046/j.1365-3121.2002.00412.x

Geshi, N., Kusumoto, S., & Gudmundsson, A. (2012). Effects of mechanical layering of host rocks on dike growth and arrest. *Journal of Volcanology and Geothermal Research*, *223–224*, 74–82. https://doi.org/10.1016/j.jvolgeores.2012.02.004

Gudmundsson, A. (1983). Form and dimensions of dykes in Eastern Iceland. *Tectonophysics*, *95*(3–4), 295–307. https://doi.org/10.1016/0040-1951(83)90074-4

Gudmundsson, A. (1995). Infrastructure and mechanics of volcanic systems in Iceland. *Journal of Volcanology and Geothermal Research*, *64*, 1–22. https://doi.org/10.1016/0377-0273(95)92782-Q

Gudmundsson, A. (2002). Emplacement and arrest of sheets and dykes in central volcanoes. *Journal of Volcanology and Geothermal Research*, *116*, 279–298. https://doi.org/10.1016/s0377-0273(02)00226-3

Gudmundsson, A., & Loetveit, I. F. (2005). Dyke emplacement in a layered and faulted rift zone. *Journal of Volcanology and Geothermal Research*, *144*(1–4), 311–327. https://doi.org/10.1016/j.jvolgeores.2004.11.027

Gudmundsson, A., & Philipp, S. L. (2006). How local stress fields prevent volcanic eruptions. *Journal of Volcanology and Geothermal Research*, *158*(3–4), 257–268. https://doi.org/10.1016/j.jvolgeores.2006.06.005

Hargraves, R. B., Johnson, D., & Chan, C. Y. (1991). Distribution anisotropy: The cause of AMS in igneous rocks? *Geophysical Research Letters*, *18*(12), 2193–2196. https://doi.org/10.1029/91GL01777

Harrison, R. J., & Feinberg, J. M. (2008). FORCinel: An improved algorithm for calculating first-order reversal curve distributions using locally weighted regression smoothing. *Geochemistry, Geophysics, Geosystems*, *9*, Q05016. https://doi.org/10.1029/2008GC001987

Hastie, W. W., Aubourg, C., & Watkeys, M. K. (2011). When an 'inverse' fabric is not inverse: An integrated AMS-SPO study in MORB-like dykes. *Terra Nova*, *23*(1), 49–55. https://doi.org/10.1111/j.1365-3121.2010.00983.x

Helgason, J., & Zentilli, M. (1985). Field characteristics of laterally emplaced dikes: Anatomy of an exhumed Miocene dike swarm in Reydarfjordur, Eastern Iceland. *Tectonophysics*, *115*, 247–274. https://doi.org/10.1016/0040-1951(85)90141-6

Hopkinson, J. (1889). Magnetic and other physical properties of iron at a high temperature. *Philosophical Transactions of the Royal Society of London A*, *180*, 443–465. https://doi.org/10.1098/rsta.1889.0014

Hrouda, F. (2011). Models of frequency-dependent susceptibility of rocks and soils revisited and broadened. *Geophysical Journal International*, *187*(3), 1259–1269. https://doi.org/10.1111/j.1365-246X.2011.05227.x

Hrouda, F., Buriánek, D., Krejčí, O., & Chadima, M. (2015). Magnetic fabric and petrology of Miocene sub-volcanic sills and dykes emplaced into the SW Flysch Belt of the West Carpathians (S Moravia, Czech Republic) and their volcanological and tectonic implications. *Journal of Volcanology and Geothermal Research*, *290*, 23–38. https://doi.org/10.1016/j.jvolgeores.2014.12.001

Hrouda, F., Faryad, S. W., Kubínová, Š., Verner, K., & Chlupácová, M. (2019). Simultaneous free flow and forcefully driven movement of magma in lamprophyre dykes as indicated by magnetic anisotropy: Case study from the central bohemian dyke swarm, Czech Republic. *Geosciences (Switzerland)*, *9*(3). https://doi.org/10.3390/geosciences9030104

Jackson, M., Gruber, W., Marvin, J., & Banerjee, S. K. (1988). Partial anhysteretic remanence and its anisotropy: Applications and grainsize-dependence. *Geophysical Research Letters*, *15*(5), 440–443. https://doi.org/10.1029/GL015i005p00440

Khan, M. A. (1962). The anisotropy of magnetic susceptibility of some igneous and metamorphic rocks. *Journal of Geophysical Research*, *67*, 2873–2885. https://doi.org/10.1029/JZ067i007p02873

Kissel, C., Laj, C., Sigurdsson, H., & Guillou, H. (2010). Emplacement of magma in Eastern Iceland dikes: Insights from magnetic fabric and rock magnetic analyses. *Journal of Volcanology and Geothermal Research*, *191*(1–2), 79–92. https://doi.org/10.1016/j.jvolgeores.2009.12.008

Knight, M. D., & Waker, G. P. L. (1988). Magma flow direction in dykes of the Koolau complex, Oahu, determined from magnetic fabric studies. *Journal of Geophysical Research*, *93*, 4301–4319. https://doi.org/10.1029/JB093iB05p04301

Kretz, R. (1983). Symbols of rock-forming minerals. *American Mineralogist*, *68*(1-2), 277–279.

Kusbach, V. K., Machek, M., Roxerová, Z., et al. (2019). Localization effect on AMS fabric revealed by microstructural evidence across small-scale shear zone in marble. *Scientific Repeports*, *9*, 17483. https://doi.org/10.1038/s41598-019-53794-y

Lanzafame, G., Iezzi, G., Mancini, L., Lezzi, F., Mollo, S., & Ferlito, C. (2017). Solidification and turbulence (non-laminar) during magma ascent: Insights from 2D and 3D analyses of bubbles and minerals in an Etnean dyke. *Journal of Petrology*, *58*(8), 1511–1534. https://doi.org/10.1093/petrology/egx063

Martin, S. A., Kavanagh, J. L., Biggin, A. J., & Utley, J. E. P. (2019). The origin and evolution of magnetic fabrics in mafic sills. *Frontiers in Earth Science*, *7*, 1–23. https://doi.org/10.3389/feart.2019.00064

Mattsson, H. B., Caricchi, L., Almqvist, B. S. G., Caddick, M. J., Bosshard, S. A., Hetényi, G., & Hirt, A. M. (2011). Melt migration in basalt columns driven by crystallization-induced pressure gradients. *Nature Communications*, *2*(1), 1–6. https://doi.org/10.1038/ncomms1298

McCabe, C., Jackson, M., & Ellwood, B. B. (1985). Magnetic anisotropy in the Trenton limestone: Results of a new technique, anisotropy of anhysteretic susceptibility. *Geophysical Research Letters*, *12*(6), 333–336. https://doi.org/10.1029/GL012i006p00333

Mollo, S., Lanzafame, G., Masotta, M., Iezzi, G., Ferlito, C., & Scarlato, P. (2011). Cooling history of a dike as revealed by mineral chemistry: A case study from Mt Etna volcano. *Chemical Geology*, *288*(1–2), 39–52. https://doi.org/10.1016/j.chemgeo.2011.06.016

Mollo, S., Putirka, K., Iezzi, G., & Scarlato, P. (2013). The control of cooling rate on titanomagnetite composition: Implications for a geospeedometry model applicable to alkaline rocks from Mt Etna volcano. *Contributions to Mineralogy and Petrology*, *165*(3), 457–475. https://doi.org/10.1007/s00410-012-0817-6

Moorbath, S., Sigurdsson, H., & Goodwin, R. (1968). K-Ar ages of oldest exposed rocks in Iceland. *Earth and Planetary Science Letters*, *4*, 197–205. https://doi.org/10.1016/0012-821x(68)90035-6

Ort, M. H., Newkirk, T. T., Vilas, J. F., & Vazquez, J. A. (2015). Towards the definition of AMS facies in the deposits of pyroclastic density currents. *Geological Society Special Publication*, *396*, 205–226. https://doi.org/10.1144/SP396.8

Paquet, F., Dauteuil, O., Hallot, E., & Moreau, F. (2007). Tectonics and magma dynamics coupling in a dyke swarm of Iceland. *Journal of Structural Geology*, *29*(9), 1477–1493. https://doi.org/10.1016/j.jsg.2007.06.001

Park, J. K., Tanczyk, E. I., & Desbarats, A. (1988). Magnetic fabric and its significance in the 1400 Ma Mealy diabase dykes of Labrador, Canada. *Journal of Geophysical Research*, *93*(B4), 13,689–13,704. https://doi.org/10.1029/jb093ib11p13689

Pike, C. R., Roberts, A. P., Dekkers, M. J., & Verosub, K. L. (2001). An investigation of multi-domain hysteresismechanisms using FORC diagrams. *Physics of the Earth and Planetary Interiors*, *126*, 11–25. https://doi.org/10.1016/s0031-9201(01)00241-2

Pike, C. R., Roberts, A. P., & Verosub, K. L. (1999). Characterizing interactions in fine magnetic particle systems using first order reversal curves. *Journal of Applied Physics*, *85*(9), 6660–6667. https://doi.org/10.1063/1.370176

Poland, M. P., Fink, J. H., & Tauxe, L. (2004). Patterns of magma flow in segmented silicic dikes at Summer Coon Volcano, Colorado: AMS and thin section analysis. *Earth and Planetary Science Letters*, *219*(1–2), 155–169. https://doi.org/10.1016/s0012-821x(03)00706-4

Porreca, M., Acocella, V., Massimi, E., Mattei, M., Funiciello, R., & De Benedetti, A. A. (2006). Geometric and kinematic features of the dike complex at Mt. Somma, Vesuvio (Italy). *Earth and Planetary Science Letters*, *245*(1–2), 389–407. https://doi.org/10.1016/j.epsl.2006.02.027

Potter, D. K., & Stephenson, A. (1988). Single-domain particles in rocks and magnetic fabric analysis. *Geophysical Research Letters*, *15*(10), 1097–1100. https://doi.org/10.1029/GL015i010p01097

Raposo, M. I. B., & Ernesto, M. (1995). Anisotropy of magnetic susceptibility in the Ponta Grossa dyke swarm (Brazil) and its relationship with magma flow direction. *Physics of the Earth and Planetary Interiors*, *87*(3–4), 183–196. https://doi.org/10.1016/0031-9201(94)02970-m

Roberts, A. P., Pike, C. R., & Verosub, K. L. (2000). First-order reversal curve diagrams: A new tool for characterizing the magnetic properties of natural samples. *Journal of Geophysical Research*, *105*, 28,461–28,475. https://doi.org/10.1029/2000JB900326

Robinson, P. T., Hall, J. M., Christensen, N. I., Gibson, I. L., Fridleifsson, I. B., Schmincke, H.-U., & Schonharting, G. (1982). The Iceland research drilling project: Synthesis of results and implications for the nature of Icelandic and oceanic crust. *Journal of Geophysical Research*, *87*(B8), 6657–6667. https://doi.org/10.1029/JB087iB08p06657

Rochette, P., Aubourg, C., & Perrin, M. (1999). Is this magnetic fabric normal? A review and case studies in volcanic formations. *Tectonophysics*, *307*(1–2), 219–234. https://doi.org/10.1016/s0040-1951(99)00127-4

Rochette, P., Jackson, M. J., & Aubourg, C. (1992). Rock magnetism and the interpretation of anisotropy of magnetic susceptibility. *Reviews of Geophysics*, *30*, 209–226. https://doi.org/10.1029/92RG00733

Rochette, P., Jenatton, L., Dupuy, C., Boudier, F., & Reuber, I. (1991). Diabase dikes emplacement in the Oman Ophiolite: A magnetic fabric study with reference to geochemistry. In T. Peters, A. Nicolas, & R. G. Coleman (Eds.), *Ophiolite Genesis and Evolution of the Oceanic Lithosphere. Petrology and Structural Geology* (Vol. 5, pp. 55–82). Dordrecht: Springer.

Schindelin, J., Rueden, C. T., Hiner, M. C., & Eliceiri, K. W. (2015). The ImageJ ecosystem: An open platform for biomedical image analysis. *Molecular Reproduction and Development*, *82*, 518–529. https://doi.org/10.1002/mrd.22489

Silva, P. F., Henry, B., Marques, F. O., Font, E., Mateus, A., Vegas, R., et al. (2008). Magma flow, exsolution processes and rock metasomatism in the Great Messejana–Plasencia dyke (Iberian Peninsula). *Geophysical Journal International*, *175*, 806–824. https://doi.org/10.1111/j.1365-246x.2008.03920.x

Silva, P. F., Marques, F. O., Henry, B., Madureira, P., Hirt, A. M., Font, E., & Loureno, N. (2010). Thick dyke emplacement and internal flow: A structural and magnetic fabric study of the deep-seated dolerite dyke of Foum Zguid (southern Morocco). *Journal of Geophysical Research*, *115*, B12108. https://doi.org/10.1029/2010JB007638

Silva, P. F., Marques, F. O., Machek, M., Henry, B., Hirt, A.m., Roxerová, Z., et al. (2014). Evidence for non-coaxiality of Ferrimagnetic and paramagnetic fabrics, developed during magma flow and cooling in a thick mafic dyke. *Tectonophysics*, *629*, 155–164. https://doi.org/10.1016/j.tecto.2014.04.017

Soriano, C., Amorós, E. B., & Crespo, M. G. (2007). Dike intrusion under shear stress: Effects on magnetic and vesicle fabrics in dikes from rift zones of Tenerife (Canary Islands). *Journal of Structural Geology*, *29*(12), 1931–1942. https://doi.org/10.1016/j.jsg.2007.08.005

Soriano, C., Beamud, E., & Garcés, M. (2008). Magma flow in dikes from rift zones of the basaltic shield of Tenerife, Canary Islands: Implications for the emplacement of buoyant magma. *Journal of Volcanology and Geothermal Research*, *173*(1–2), 55–68. https://doi.org/10.1016/j.jvolgeores.2008.01.007

Soriano, C., Beamud, E., Garcés, M., & Ort, M. H. (2016). "Anomalous" magnetic fabrics of dikes in the stable single domain/superparamagnetic threshold. *Geophysical Journal International*, *204*(2), 1040–1059. https://doi.org/10.1093/gji/ggv495

Stephenson, A. (1994). Distribution anisotropy: Two simple models for magnetic lineation and foliation. *Physics of the Earth and Planetary Interiors*, *82*(1), 49–53. https://doi.org/10.1016/0031-9201(94)90101-5

Tarling, D. H., & Hrouda, F. (1993). *The magnetic anisotropy of rocks*. London: Chapman & Hall.

Trippanera, D., Urbani, S., Kissel, C., Winkler, A., Sagnotti, L., Nazzareni, S., et al. (2020). *Magnetic susceptibility and thin sections data from the Alftafjordur volcanic system in Eastern Iceland*. Potsdam, Germany: GFZ Data Services. https://doi.org/10.5880/fidgeo.2020.026

Urbani, S., Trippanera, D., Porreca, M., Kissel, C., & Acocella, V. (2015). Anatomy of an extinct magmatic system along a divergent plate boundary: Alftafjordur, Iceland. *Geophysical Research Letters*, *42*(15), 6306–6313. https://doi.org/10.1002/2015GL065087

Walker, G. P. L. (1960). Zeolite zones and dyke distribution in relation to the structure of the basalts of Eastern Iceland. *Journal of Geology*, *68*, 515–528. https://doi.org/10.1086/626685

Walker, G. P. L. (1974). The structure of Eastern Iceland. In L. Kristjansson (Ed.), *Geodynamics of Iceland and the North Atlantic Area. NATO Advanced Study Institute Series, Iceland, 1–7 July 1974*, *Series C—Mathematical and Physical Sciences* (Vol, 11, pp. 177–188). Dordrecht, The Netherlands: Springer. https://doi.org/10.1007/978-94-010-2271-2_12

References From the Supporting Information

Jackson, M., Moskowitz, B., Rosenbaum, J., & Kissel, C. (1998). Field-dependence of AC susceptibility in titanomagnetites. *Earth and Planetary Science Letters*, *157*(3–4), 129–139. https://doi.org/10.1016/s0012-821x(98)00032-6